Frontiers in Scientific Research and Technology

Online ISSN: 2682-2970
Print ISSN: 2682-2962
http://fsrt.journals.ekb.eg

FSRT J 7 (2023) 70 - 96 10.21608/FSRT.2023.229137.1102

Assessing Geotechnical Property for Construction Purposes: A Study on the Efficacy of Shallow Seismic Refraction Tomography Method

Mariam Qaher[1], Ahmed M. Eldosouky[1], Saada A. Saada[1], Alhussein Adham Basheer[2]

[1] Geology Department, Faculty of Science, Suez University, Suez 43518, Egypt

[2] Geology Department, Faculty of Science, Helwan University, 11790 Cairo, Egypt.

ARTICLE INFO

Article history:
Received 16 August 2023
Received in revised form 14 September 2023
Accepted 16 September 2023
Available online 24 September 2023

Keywords

Seismic refraction tomography (SRT), Elastic moduli, Geotechnical parameters, Foundation bearing capacities.

ABSTRACT

The seismic refraction tomography (SRT) method, which is environmentally compatible was used to evaluate the in situ geotechnical properties of rocks in El Alamein, a new city of northwestern Egypt. SRT data were obtained along nine profiles. The results of primary wave velocities (Vp), which are 400 to 1000 m/sec for the first layer, 700 to 1250 m/sec for the second layer, and 550 to 1150 m/sec for the third layer, and secondary wave velocities (Vs), which are 150 to 330 m/sec for the first layer, 230 to 430 m/sec for the second layer, and 170 to 390 m/sec for the third layer, were correlated with the data extracted from nine boreholes drilled within the study area. The elastic moduli (kinetic rigidity, modulus, young modulus, and bulk modulus) and the geotechnical characteristics like Poisson's ratio, stress ratio index, concentration index, material index, N value, density gradient, and bearing capacity of the foundation materials were calculated from the propagation velocities of the different types of seismic waves. These elements were combined to determine the most suitable site for construction. The area can be categorized based on cohesive layer thickness, soil cohesion from geotechnical properties, and proximity to test wells into two regions: (1) unfit for construction due to weak soil cohesion caused by seawater intrusion and thin buildable layers, (2) suitable for construction at one or two levels, with strong soil cohesion, thicker buildable layers, and less noticeable seawater interference.

1. Introduction

The North Coast of Egypt is a fast-expanding coastal region along the Mediterranean Sea. El-Alamein New City is located on Egypt's northern shore, some 240 kilometers (150 miles) west of Alexandria. It is strategically located with a view of the Mediterranean Sea. The North Coast is well-known for its beautiful beaches, opulent resorts, and affluent holiday spots. It has grown in popularity as a tourist attraction for both domestic and foreign visitors, particularly during the summer months.

In the current research, a notable knowledge gap exists regarding the comprehensive evaluation of the elastic moduli and geotechnical properties of rocks in the specific context of the study area. While prior studies may have touched upon certain aspects of these properties (Qaher et al., 2023), a holistic understanding of the interplay between cohesive layers, soil cohesion, and the intrusion of seawater in this region remains limited.

This study aims to bridge this gap by providing a thorough examination of the integration between all these critical factors and their implications for construction suitability. Various methods have been employed in the past to determine the geotechnical properties of rocks. These methods include but are not limited to, laboratory testing, Cone Penetration Testing (CPT), Standard Penetration Testing (SPT), Spectral Analysis of Surface Waves (SASW), and Downhole Logging Surface Roughness Techniques (Koukis et al., 2007; Samui and Sitharam, 2010). These methods offer a promising alternative to traditional approaches, especially in areas with potential seawater intrusion but they provide limited subsurface information (Cosenza et al., 2006; Hubbard, 2009; Al-Heety et al., 2021). While each of these methods has its merits, SRT holds promise in the study due to its non-invasive nature, cost-effectiveness, and potential to evaluate soil cohesion in the presence of seawater intrusion more effectively. The preference for SRT is based on its suitability to provide a comprehensive analysis of geotechnical properties to better inform construction decisions in the study area.

In the present research, the data obtained from nine SRT profiles are used to calculate P-wave (VP) and S-wave (VS) velocities. The lithological information is also

* Corresponding author at Suez University

E-mail addresses: Mariam.Qaher@sci.suezuni.edu.eg (Mariam Qaher)

obtained from nine drilled boreholes in the study area on the North Coast (Fig. 1). Then for direct information regarding the quality of the soil or rock materials, the elastic moduli (kinetic rigidity, modulus, young modulus, and bulk modulus), geotechnical parameters (material index, Poisson's ratio, concentration index, stress ratio, N value, and density gradient), bearing capacities (Ultimate and allowable) can be used.

The primary aim of this investigation is to utilize Seismic Refraction Tomography (SRT) as an effective tool not only to determine layer velocities and thicknesses but also to conduct engineering assessments and evaluate the geotechnical characteristics of rocks and sediments in the study area. Based on the analysis of Seismic Refraction Tomography (SRT) data and subsequent geotechnical assessments, the study anticipates the expected results of zonal Classification, construction Suitability, risk mitigation, improved Engineering, and enhanced geotechnical practices. Generally, this investigation aims to provide a robust understanding of the geotechnical characteristics of the study area, facilitating informed decisions for construction and engineering projects, and ultimately contributing to the development of safe, durable, and reliable infrastructure in the region.

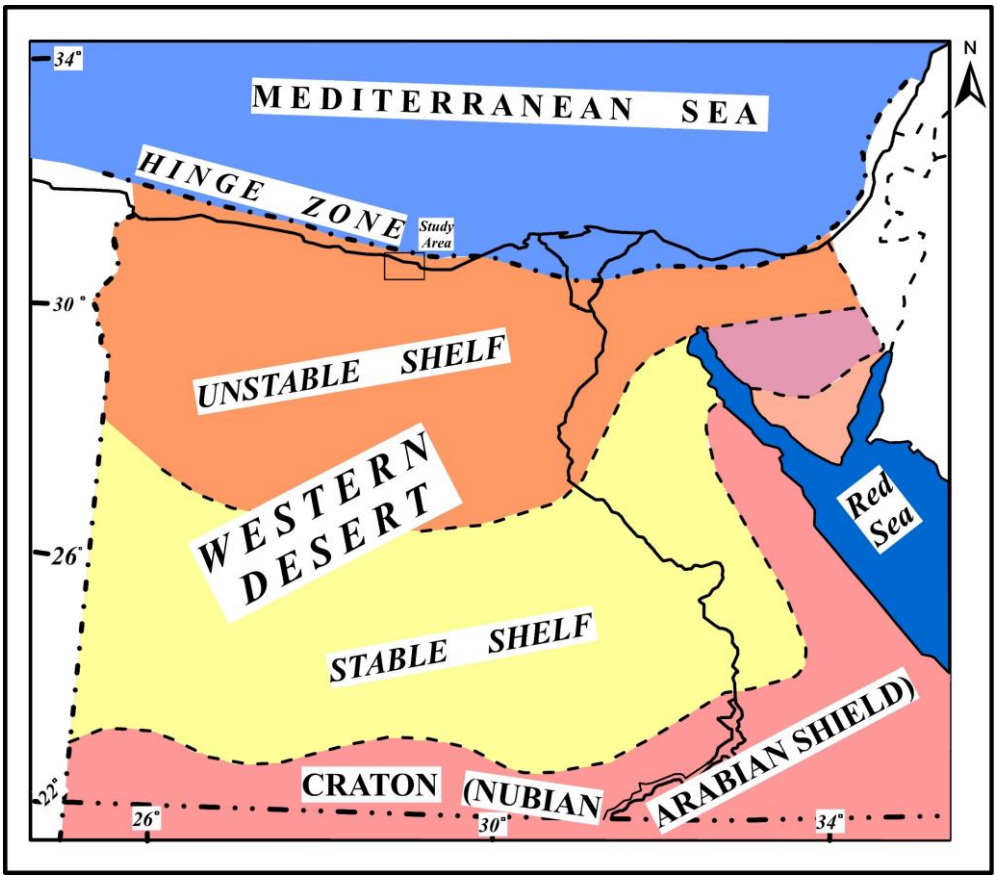

Figure 1: A Sketch of Egypt's structural aspects with the study area is shown as a black-framed rectangle (after Schlumberger, 1984).

2. Geologic setting

The stratigraphic link between Tertiary and Quaternary strata and the top surface deposits within the coastal region can be seen in Figure (2), which serves as the focus of our research (Shukri et al., 1956; Butzer, 1960; Said, 1962; Atwa, 1979; Said, 1990). The following section provides a chronological overview of these stratigraphic units, commencing with the earliest:

I. Pliocene El Hagif Formation: This layer consists of fissured limestone at the surface and calcareous sandstone at the base (Said, 1990; Yousif et al., 2013).

II. Pleistocene Kurkar Ridges or Alexandrian Formation: Mainly composed of oolitic limestone and is characterized by two elongated inland and foreshore ridges that run parallel to the coast and are separated by longitudinal depressions (Hume and Hughes, 1921; Shukri et al., 1956; Butzer, 1960; Hammad, 1966; Shata, 1971).

III. Holocene Sediments: The Holocene sediments encompass a range of deposits as outlined by Abu Risha and Sturchio (2018):

(i) Beach deposits consist of oolitic sand, quartz sand, and shell fragments.

(ii) Aeolian deposits covering oolitic limestone ridges along the shore.

(iii) "Sabkha deposits" refer to the region below sea level, which experiences seasonal fluctuations in seawater. These deposits predominantly comprise aeolian sand

bound together by salts resulting from seasonal water evaporation.

(iv) Alluvial deposits fill the channels of drainage lines and elongated depressions between the ridges in the coastal plain (Said, 1990; Shaaban, 2004).

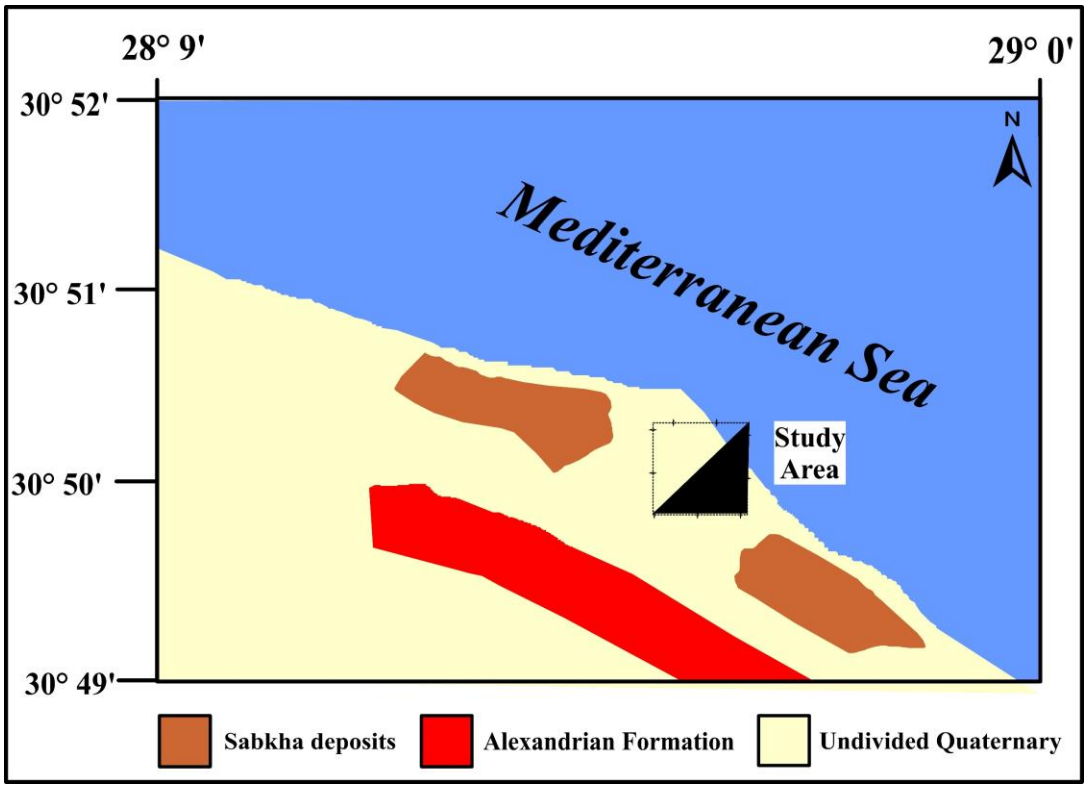

Figure 2: Geological setting of the study area (after Basheer and Salama 2022).

The North Coast of Egypt, which runs along the Mediterranean Sea, has a simpler geological structure than the rest of Egypt, which is dominated by the Nile Delta and the Sinai Peninsula. Faults and folds are geological phenomena on the North Coast, but they are not as prominent or complicated as in other sections of Egypt. Egypt has various fault systems; however, they are less prominent near the North Coast than in other areas. These faults are the product of tectonic processes that shaped the Mediterranean area. The North Coast lies on the border between the African Plate and the Eurasian Plate (Saleh et al., 2006), which causes some faulting and seismic activity, albeit not as strong as in other sections of the nation. These faults, which are related to earthquakes and the creation of tiny basins and structural highs, can have a considerable influence on the region (Iskander, 2013; Iskander, 2021).

The North Coast of Egypt has some fold structures as well, albeit they are not as prominent as in other geological contexts. When opposed to locations with active mountain-building processes, fold structures in this region are usually soft, wide, and less complicated. In recent geological history, the Mediterranean Sea has remained tectonically stable, limiting the formation of large-scale folding (Elstohey et al., 2023).

The Nile Delta dumps a large quantity of silt along this shoreline, resulting in sandy beaches, dunes, and shallow coastal regions. The prevailing sea currents and wind patterns frequently impact these deposits. The North Coast is undergoing continuing coastal erosion and deposition processes because of wave action and longshore drift. These processes can shape the shoreline over time and help to generate coastal landforms (Dewidar et al., 2010; Salem et al., 2013).

Nine exploratory boreholes have been drilled in the study area (Fig. 3). Depending on the data from the boreholes, the study area is generally underlain by sandy soil with different saturation levels. The surface layer is composed of dry beach sand. Its thickness varies from 16.1 meters as observed in well 3 (near the seacoast) and decreases as we move far from the seacoast to 6.89 meters as observed in well 7. The second layer is composed of nearly wet silty sand. Its thickness varies from 18.44 meters as observed in well 1 (near the seacoast) to 2.32 meters as observed in well 4. The third layer is composed of sand saturated with seawater. Its thickness varies from 18.44 meters as observed in well 1 (near the seacoast) to 2.32 meters as observed in well 4 (Fig. 4).

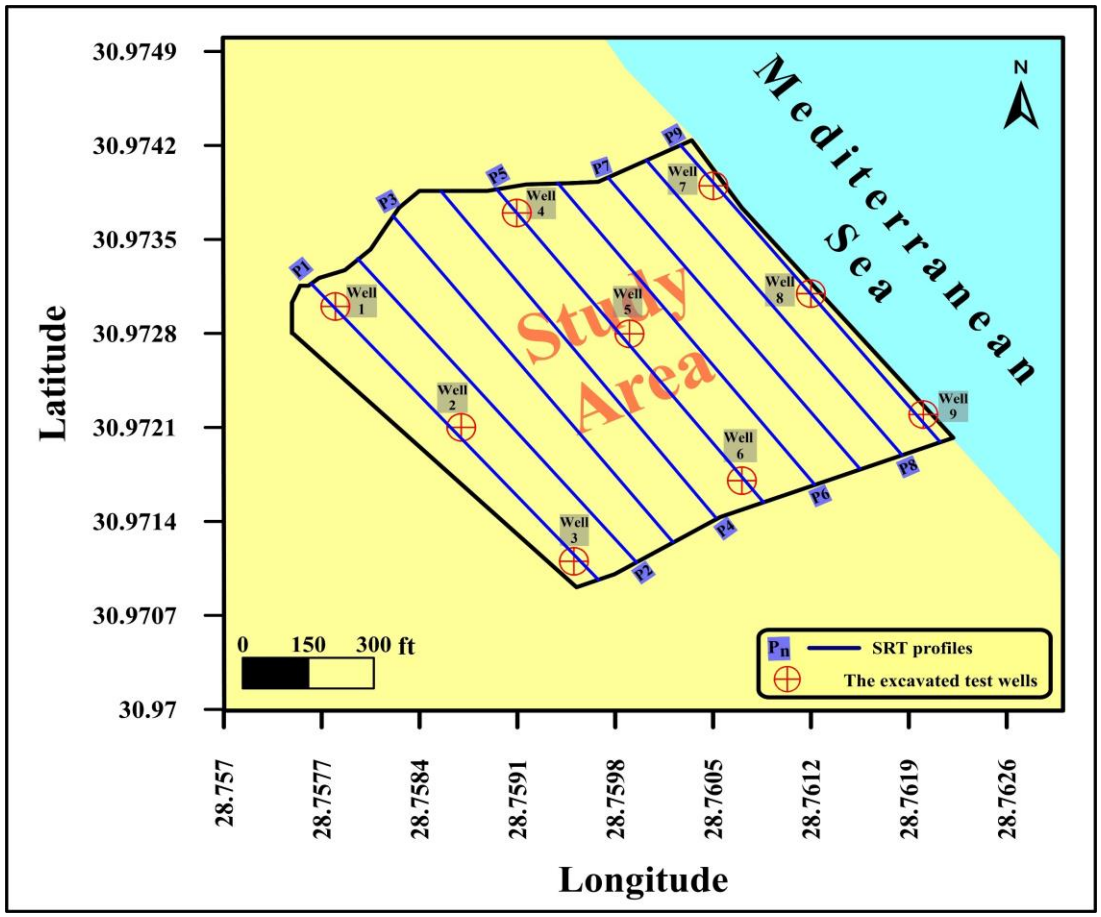

Figure 3: The location of SRT profiles and boreholes.

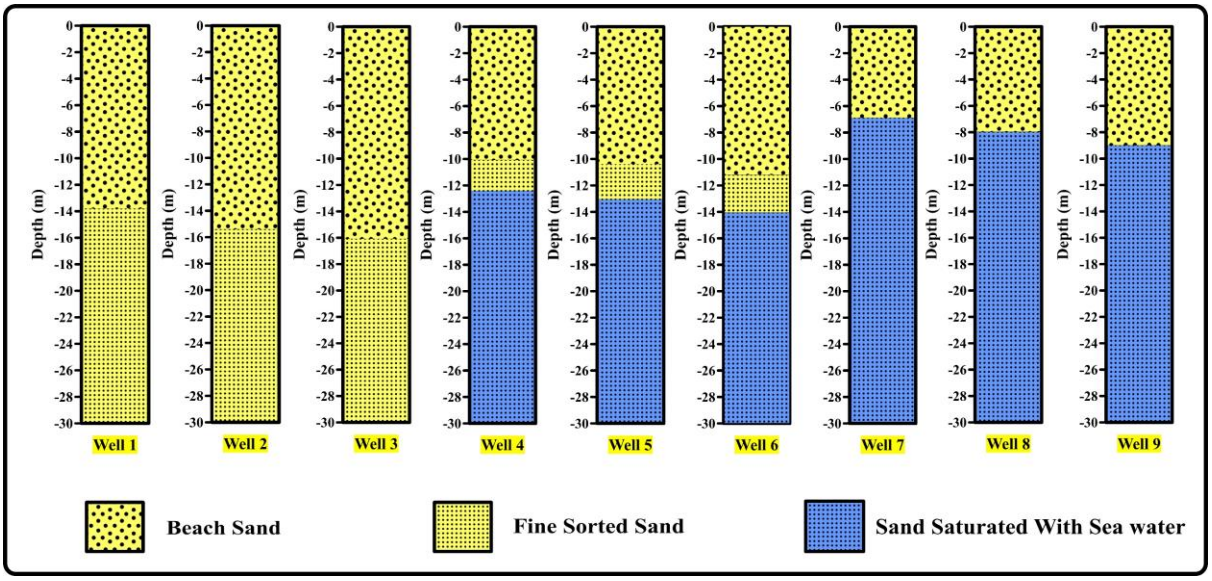

Figure 4: Drilled Boreholes.

3. Methodology

3.1. SRT data acquisition

In the methodology employed for this study, a controlled seismic source was employed to emit seismic waves, which subsequently propagated into the Earth's subsurface. Within the subsurface, some of these waves underwent either reflection or refraction at geological interfaces before returning to the Earth's surface. These returning waves induced ground motion, which was meticulously recorded by strategically placed geophones at the surface. The primary purpose of this recording was to precisely measure the arrival times of the waves at varying distances from the seismic source. Subsequently, the collected travel time data underwent mathematical transformations to derive depth values. This transformation process enabled the systematic mapping of the distribution of subsurface geological interfaces (Dobrin, 1976; Kearey et al., 2002). It is noteworthy that, in the refraction method utilized, only the initial arrivals of the seismic waves were recorded, primarily represented by either direct or refracted rays (Sharma, 1997).

To conduct the survey, a specialized equipment called "Geometrics, Smartseis" was employed. The survey was conducted using the in-line spread configuration. In this configuration, the geophone array was positioned on the ground, following an uninterrupted horizontal path that traversed the shot point. Additionally, three different shot point locations, including Normal, middle, and reverse orientations, were employed along each of the nine profiles. These profiles were directed in a northwest-to-southeast orientation, parallel to the Mediterranean Sea (Fig. 3).

3.2. Interpretation of SRT data

The result of shallow seismic refraction measurements was compared with drilled boreholes in the study area in terms of the number of layers, thickness, and lithology. SRT data and drilled boreholes demonstrate the existence of three layers in the study area. The velocities of both P-wave and S-wave of these layers are calculated and given in Table (1).

Table 1: P-and S-wave velocities of dry, silty, and saturated sand.

Layers	Vp (meters/second)	Vs (meters/second)
The top layer (Dry sand)	400 to 1000	150 to 330
The second layer (nearly wet silty sand)	700 to 1250	230 to 430
The third layer (Saturated sand)	550 to1150	170 to 390

3.3. Elastic moduli

Measuring the in-situ elastic dynamic modulus can be a challenging and costly endeavor. Therefore, researchers and fieldwork experts have sought alternative methods to calculate these moduli with less cost and greater efficiency. In this study, various relationships will be used to calculate the elastic moduli using seismic wave velocities and the density of the material, providing a more practical and economical approach (D'Andrea et. al., 1965; Potter and Fottinek, 1997; AL-Zubedi, 2020). After that, contour maps have been generated for multiple layers to illustrate the distribution of elastic moduli across the area under investigation.

3.3.1. Kinetic Shear Modulus (μ)

Kinetic Shear Modulus is defined as the ratio between shear stress and shear strain (Dobrin, 1976). Ideal liquids and gases can't be subjected to shear stress; accordingly, this modulus equals zero (μ=0). It is an important engineering characteristic of sediments or soils. This modulus value is easily calculated from shear wave velocity (V_s) with the help of the bulk density (ρ) (Toksöz et al., 1976; Khalil and Hanafy, 2016) as follows:

$$\mu = \rho V_s^2 \quad (1)$$

The shear strength increases with increasing effective pressure (Hamilton, 1971; Sharma, 1997). In an engineering study, porosity and water saturation are important factors affecting rigidity (Hardin and Dmevich, 1972). They observed that the decrease in this modulus is a product of higher porosities whereby the effect of water saturation is small. Biot (1956) and Kuster and Toksoz (1974) found that this modulus remains constant or increases only slightly as the rock is saturated with fluid.

3.3.2. Kinetic Young's Modulus (E)

Kinetic Young's Modulus is specified as the ratio of normal stress to normal strain (Dobrin, 1976). It can be obtained from the law of Imai (1975) based on shear modulus (μ) and Poisson's ratio (σ) in this manner:

$$E = 2\mu(1+\sigma) \quad (2)$$

Young's modulus generally behaves as a bulk modulus i.e., it also depends on the variations in porosity, fluid saturation, and pressure (Salem, 1990). Rahmouni et al. (2017) concluded that slow increase of elastic moduli up to

80 % of saturation and for great overload by liquid, both the bulk modulus and Young's modulus quickly rise.

3.3.3. Kinetic Bulk Modulus (K)

Kinetic Bulk Modulus is also known as incompressibility and is calculated by dividing the stress by the proportionate change in volume or it depicts the volume change of components exposed to all forces as compressive and decompression resistances. The use of the following equation, we can calculate the different values of this modulus for the three layers based on Young's modulus (E) and Poisson's ratio (σ) (Abd Elrahman, 1989; Mott et al., 2008):

$$\mathbf{k} = (\mathbf{E})/(3\ (1 - 2\ \boldsymbol{\sigma})) \quad \textbf{(3)}$$

Geertsma (1961) pointed out that rock compressibility (inverse of the bulk modulus) is a function of the porosity, grain size distribution, composition of cementing material, type of sediments, and effective stress. He concluded that lower compressibility or high bulk modulus corresponds to higher confining pressures and, consequently, to lower porosities. This modulus is highly affected by water saturation (Biot, 1956; Nur and Simons, 1969; Kuster and Toksoz, 1974). Gregory (1976) concluded that the elastic moduli decrease as porosity increases.

3.4. Geotechnical parameters

Shallow seismic refraction is an efficient method for quickly identifying the geotechnical parameters in engineering and construction projects (Almalki et al., 2011; Khalil and Hanafy, 2016; Khorshid, 2016; Abudeif et al., 2017; Adewoyin et al., 2017; Shebl et al., 2019; Momoh et al., 2020; Ghanem et al., 2021). The ground's soil is the only building material with more changeable engineering and physical characteristics that vary both laterally and vertically (Bowles, 1982). Some of the shallow parameters were estimated and integrated to assess the competence and suitability of the subsurface layers for building and to choose the most appropriate zone for construction.

3.4.1. Poisson's Ratio (σ)

Poisson's ratio is important in the elastic field. It has no unity and represents the change in the geometric shape of the material. It is defined as "the ratio of lateral contraction strain for each unit breadth divided by longitudinal extension strain for each unit length" when the affected stress lies within the limits of elasticity (Sheriff, 1991). This ratio approaches zero for very hard indurate rocks (for example in granite σ ≈ 0.05), while in fine sediments with weak cohesion, this ratio increases to 0.49, and if it equals 0.5, rocks behave like fluids (Salem, 1990; Telford et al., 1990; Gretener, 2003) so the less competent material is, the higher the values of **Poisson's ratio** are, and vice versa (Telford et al., 1990). The next equation is applied to determine the values of this ratio in relationship with P-wave (V_p) and S-wave (V_s) velocities (Sjogren, 1984; Telford et al., 1990):

$$\boldsymbol{\sigma} = \left(1 - 2\left(\frac{V_s}{V_p}\right)^2\right) \Big/ \left(2 - 2\left(\frac{V_s}{V_p}\right)^2\right) \quad \textbf{(4)}$$

3.4.2. N-value

N-value is referred to as the resistance to penetration or the number of blows required to penetrate the soil by normalized cylindrical bars under a standard load and carried out on-site. High-competent materials have high penetration resistance or high N which means it is hard to penetrate it and vice versa. For sand, clay, silt, or other known types of soil/sediment, shear wave data may also be mathematically transformed to N-values for use in calculating bearing capacities (Othman, 2005). Using the modified Imai's (1975) equation to calculate the N-values by Stumpel et al. (1984):

$$V_s = 89.9\ N^{0.341} \quad \textbf{(5)}$$

According to Bowles (1984), the values for cohesive soil are arranged as follows: below 4 (very soft sediments), 4-6 (soft materials), 7-15 (medium dense), 16-25 (stiff), and above 25 (hard rock). For cohesionless soil: 0-10 (loose), 11-30 (medium), 31-50 (dense), and above 50 (very dense).

3.4.3. Material Index (M_i)

Material Index is one of the most essential characteristics that may be derived based on the seismic refraction survey results. It clarifies the foundation-related material quality and serves as a gauge for a material's degree of hardness or competence (Abd Elrahman, 1989). According to Abd Elrahman (1989), this index can be obtained by:

$$\mathbf{M}_i = 1 - 4\ \boldsymbol{\sigma} \quad \textbf{(6)}$$

This index is influenced by the minerals of the rock or soil as well as the physical environment to which it is exposed which affects the wave velocity by influencing the level of consolidation, fracturing, jointing, and the existence or nonexistence of liquids in pore spaces (Das, 1994). In general, according to Abd Elrahman (1989), this index ranges from +1 for highly competent or very hard indurated material to -1 for low competent or soft material. Rocks are classified in terms of hardness into four main groups for building and construction purposes (Birch, 1966; Gassman, 1973; Tatham, 1982; Sheriff and Geldart, 1986). This classification is very important in the field of civil engineering to determine the type of foundations for buildings. Large buildings need solid rocks to support their foundations (Al-Heety, 2014; AL-Zubedi, 2020).

The first group, in which the values lie, is the group in which the material index value ranges between -1 to -0.5 and includes recent sediments of rivers, winds, and volcanic ash, where these deposits are characterized by being of little to no hardness. The value of the Poisson's ratio for these deposits ranges between 0.36 to 0.5. Some types of these sediments that have a Poisson's ratio of 0.5 behave like a liquid when exposed to high pressure, which makes them unsuitable from an engineering point of view. This group reflects incompetent to slightly competent materials. The second group is the group in which the material index value ranges between -0.5 to 0, and it represents rocks and sediments of medium hardness and high porosity, such as river deposits, and carbonate rocks

that contain cracks, fractures, and caves. These rocks and sediments are characterized by the value of the Poisson's ratio ranges between 0.35 to 0.26. This group reflects fairly to moderately competent materials. The third group is the group in which material index value ranges between 0 to 0.5, and it represents non-porous rocks of high hardness, such as carbonate rocks, and some types of metamorphic and igneous rocks. These rocks are characterized by the value of Poisson's ratio between 0.16 to 0.25. This group reflects competent materials. The fourth group is the group in which the material index value ranges between 0.5 to +1, and it represents non-porous rocks of very high hardness, such as sandy rocks, metamorphic rocks, and igneous rocks. The value of Poisson's ratio ranges from 0.15 to 0. This group reflects very highly competent materials (AL-Zubedi, 2020).

3.4.4. Concentration Index (C_i)

This index is also called the competence index and referred to as the level of expertise for foundation and additional civil engineering applications. The value of C_i at shallow depths is confined between 3 to 6. It is greater than 6 for hard rocks and the value of C_i of the soft and non-hardened sediments that behave like the behavior of liquids when exposed to pressure is 3. This index is inversely related to stress ratio and there is a direct relation between this index, material index, N value, and rock hardness (Abd Elrahman, 1991). The following equation is used to calculate this index (Bowles, 1982):

$$C_i = \frac{(1+\sigma)}{\sigma} \quad (7)$$

Abd Elrahman (1991) defines this index in terms of P- and S-wave velocities (V_P and V_S):

$$\mathbf{C}_i = \left[3 - 4\left(\frac{V_s^2}{V_p^2}\right)\right] \Big/ \left[1 - 2\left(\frac{V_s^2}{V_p^2}\right)\right] \quad (8)$$

3.4.5. Stress Ratio Index (Si)

Stress Ratio Index (Si) is defined as the ratio between the horizontal stress as a result of the pore-filling fluids and vertical stress at a certain depth (Hunt, 1986). This ratio decreases as overburden pressure or depth increases. Bowles (1982) noted that this ratio is low for coarser soils and high for finer soils and it increases as depth or overburden pressure decreases. This index ranges from 0.25 to 0.70 as the small values indicate hard, low porosity, and more competent materials and vice versa. This ratio and Poisson's ratio exhibit the same behavior as it increases for the high-water content less hard materials (Al-Fahdawi, 2000).

A sensitive scale that divides soils into soft, fairly compacted, moderately compacted, and compacted categories can be introduced using the stress ratio (Abd Elrahman, 1989). Bowles (1982) and Thomsen (1986) described a relationship to calculate this index as follows:

$$\mathbf{S_i} = S_{horizontal}/S_{vertical} = \sigma/(1-\sigma) \quad (9)$$

Other relations are expressed by Abd Elrahman (1991) to calculate this ratio:

$$\mathbf{S_i} = 1 - 2\left(\mathbf{V}_s^2/\mathbf{V}_p^2\right) \quad (10)$$

3.4.6. Density Gradient (Di)

The physical process by which sediments are converted from their original condition to a gradually denser condition as an outcome of their weight or tectonic movements is referred to as compaction (Cordier, 1985). This gradient links to the level value of consolidation or settlement that will occur and is defined according to Stumpel et al. (1984):

$$\mathbf{D_i} = \left[\mathbf{V_p^2} - 4/3\mathbf{V_s^2}\right]^{-1} \quad (11)$$

When a slight change in pressure on soil decreases the porosity and increases the density from the initial state, this means that the soil is soft, and the result of this gradient is high. Alternatively, minimum values of density gradient can be predictable in hardened rock.

3.5. Foundation Bearing capacities

It is the capacity of the rock, soil, or foundation material to securely bear loads without shear (Terzaghi, 1943) and a gauge for the structural stability of the soil (Lowrie, 2007).

3.5.1. Ultimate bearing capacity (Q_{ult})

It is described as the highest-limit load necessary to fracture or break it (Abd Elrahman et al., 1992). When designing engineering constructions, the quantity (Q_{ult}) is calculated because if the generated load is higher than soil capacity, distortion and creep of the layers occur, which leads to engineering problems such as settlement (Bowles, 1984). The ultimate bearing capacity of the cohesionless soils using the SPT can be evaluated by Parry's (1977) formula as:

$$\mathbf{Q_{ult}} = \mathbf{30N} \quad (12)$$

3.5.2. Allowable bearing capacity (Q_a)

When all pertinent factors are considered that ensure sufficient safety against soil mass rupture, it is described as the maximum pressure that may be acceptable on foundation soil (Abd Elrahman et al., 1992). It is determined by dividing the ultimate capacity values (Q_{ult}) by a safety factor (FS) that equals two when the soil is cohesionless and equals three when the soil is cohesive, according to Parry (1977):

$$\mathbf{Q_a} = \mathbf{Q_{ult}}/\mathbf{FS} \quad (13)$$

The safety factor (FS) equals 2 when the soil is cohesionless and equals 3 when the soil is a cohesive material.

4. Results and discussion

4.1. Layer velocities and thicknesses

4.1.1. Primary wave velocities (Vp)

The horizontal distribution of P-wave velocity for all layers is shown in Figure (5). The maximum values are in the southwestern part of the dry sand (top) and the silty sand (second) layers and in the northwestern, western, and southwestern parts of the third layer of the study area. These values decrease gradually toward the northeastern part of all layers, the eastern part of the first and third layers, and the southeastern part of the third layer.

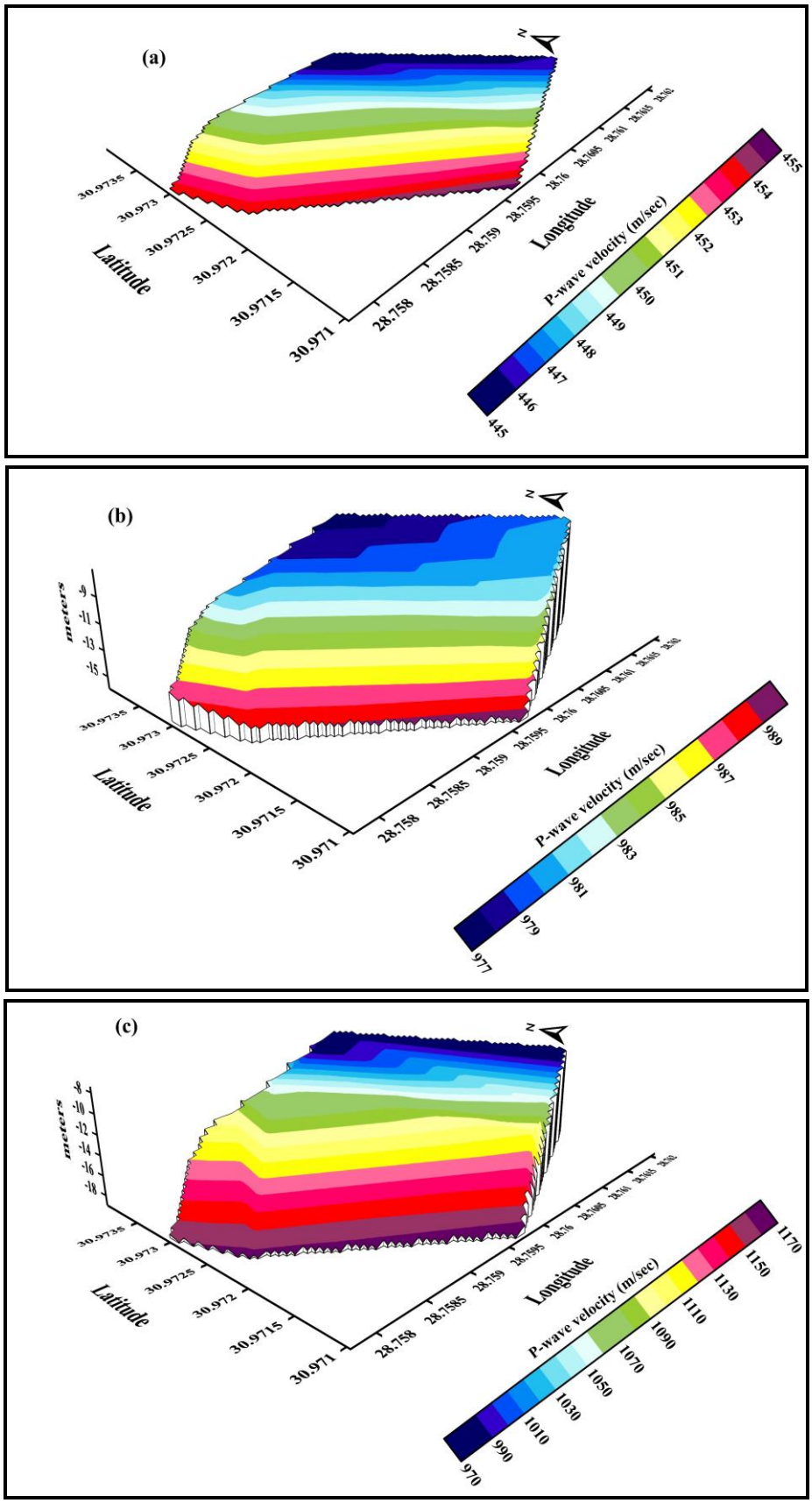

Figure 5: Vp distribution for (a) top (b) second (c) third layers.

4.1.2. Secondary wave velocities (Vs)

The horizontal distribution of S-wave velocity for all layers is shown in Figure (6). The maximum values are in the southwestern part of all layers, and the northwestern and western parts of the third layer. These values decrease gradually toward the northeastern part of all layers, the eastern part of the top and third layers, and the southeastern part of the third layer.

4.1.3. Layer thickness

The maximum thickness is observed in the southwestern part of the dry sand (top) layer (Fig. 7a) and the northwestern side of the silty sand (second) layer (Fig. 7b). These values decrease toward the northeast, east, and southeast directions of the top layer and the northeast direction of the silty sand (second) layer.

4.2. Elastic moduli

4.2.1. Kinetic Shear Modulus (μ)

The distribution of the shear modulus values for all layers is shown in Figure (8). The lowest values for the three layers are observed in the southwestern, western, and northwestern parts and steadily increase into the northeastern, eastern, and southeastern parts of the study area.

4.2.2. Kinetic Young's Modulus (E)

The Young's modulus values of the dry sand (Fig. 9a) are lower than that of nearly wet silty sand (Fig. 9b) and the sand saturated with seawater (Fig. 9c) has the highest values. In other words, with an increase in the saturation level of the layers from dry sand to nearly wet silty sand to saturated sand, the values of Young's modulus increase in the same sense as Gregory (1976) and Rahmouni et al. (2017). The low values for the three layers are detected in the southwestern, western, and northwestern sides of the investigated region, and increase gradually to the middle of the study area until reach their maximum values in the northeastern, eastern, and southeastern sides.

4.2.3. Kinetic Bulk Modulus (K)

The distribution of bulk modulus values for the first dry sand (Fig. 10a), second nearly wet silty sand (Fig. 10b), and third saturated sand (Fig. 10c) layers. The minimum values of this modulus for the three layers are observed in the northwestern, western, and southwestern parts of the investigated region. The lowermost values are in the northwestern corner. These values increase gradually toward the northeast, east, and southeast directions. The maximum values are observed in the southeastern corner of the study area.

4.3. Geotechnical Parameters

4.3.1. Poisson's Ratio (σ)

The distribution of this ratio for the three layers is shown in Figure (11). In general, the three layers show slight changes that are almost constant and nearly have high values of about 0.43 to 0.44 that reflect the low competent materials with a very low bearing capacity (Salem, 1990; Telford et al., 1990; Gretener, 2003**;** AL-Zubedi, 2020**).** The highest values are observed in the southwestern parts for all layers and in the western part of the third layer and decrease gradually toward the northeastern parts of all layers and in the eastern and southeastern parts of the third layer.

4.3.2. N value

For the top layer (Fig. 12a), these values range from 4.57 in the northern, northeastern, eastern, and southeastern corners to 4.87 in the southwestern, western, and northwestern corners of the studied area that reflect soft loose soil (Bowels, 1984). For the silty sand (second) layer (Fig. 12b), the N-values vary from 44.61 in the northern, northeastern, eastern, and southeastern corners to 46.36 in the southwestern, western, and northwestern corners which, according to Bowles (1984), reflects hard and dense competent soil. For the saturated sand (third) layer (Fig. 12c), these values range between 44.6 and 75.4 which, according to Bowles (1984), reflect the lateral change from hard dense competent soil in the northeastern, eastern, and southeastern corners to very hard dense soil in the southwestern, western, and northwestern corners.

4.3.3. Material Index (M_i)

The change is very small (-0.74 to -0.75), and it is almost constant. The low values of the material index for the three layers exist in the southwestern, western, and northwestern parts and increase with very small values in the northeastern, eastern, and southeastern parts of the study area. The material index values reach their maximum in the northeastern corner of the study area for the three layers, the eastern part of the top layer, and the southeastern corner of the third layer (Figs. 13 a-c). Generally, most of the region has very low values that reflect, according to AL-Zubedi (2020), slightly competent materials.

4.3.4. Concentration Index (C_i)

In general, the concentration index values in the study area are very close and small about 3.29 because the entire area is composed of a sand component with a different water saturation and the slight differences due to the overlapping of other materials like clay and silt, a variation in the size of the sand grains, or an increase in the perpendicular load on the lower layers (Basu et al. 2008; Shipton and Coop, 2015; Gupta and Basu 2017; Basheer and Salama, 2022). The low values are detected in the southwestern, western, and northwestern parts of the investigated region and increase gradually to the middle part until reaching maximum values in the east, and the northeastern portions of the investigated region (Fig. 14), this indicates a less competent material.

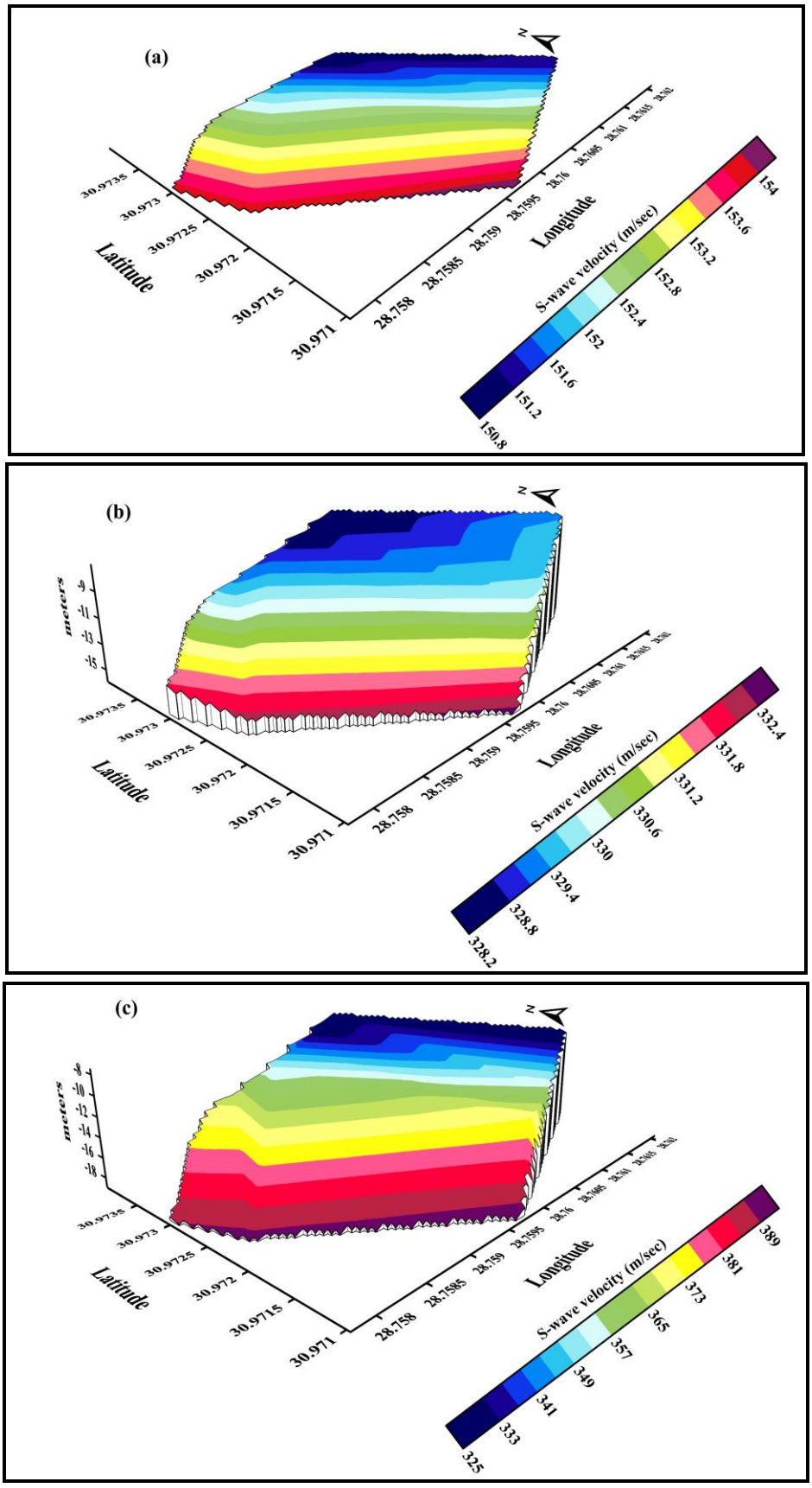

Figure 6: Vs distribution for (a) top (b) second (c) third layers.

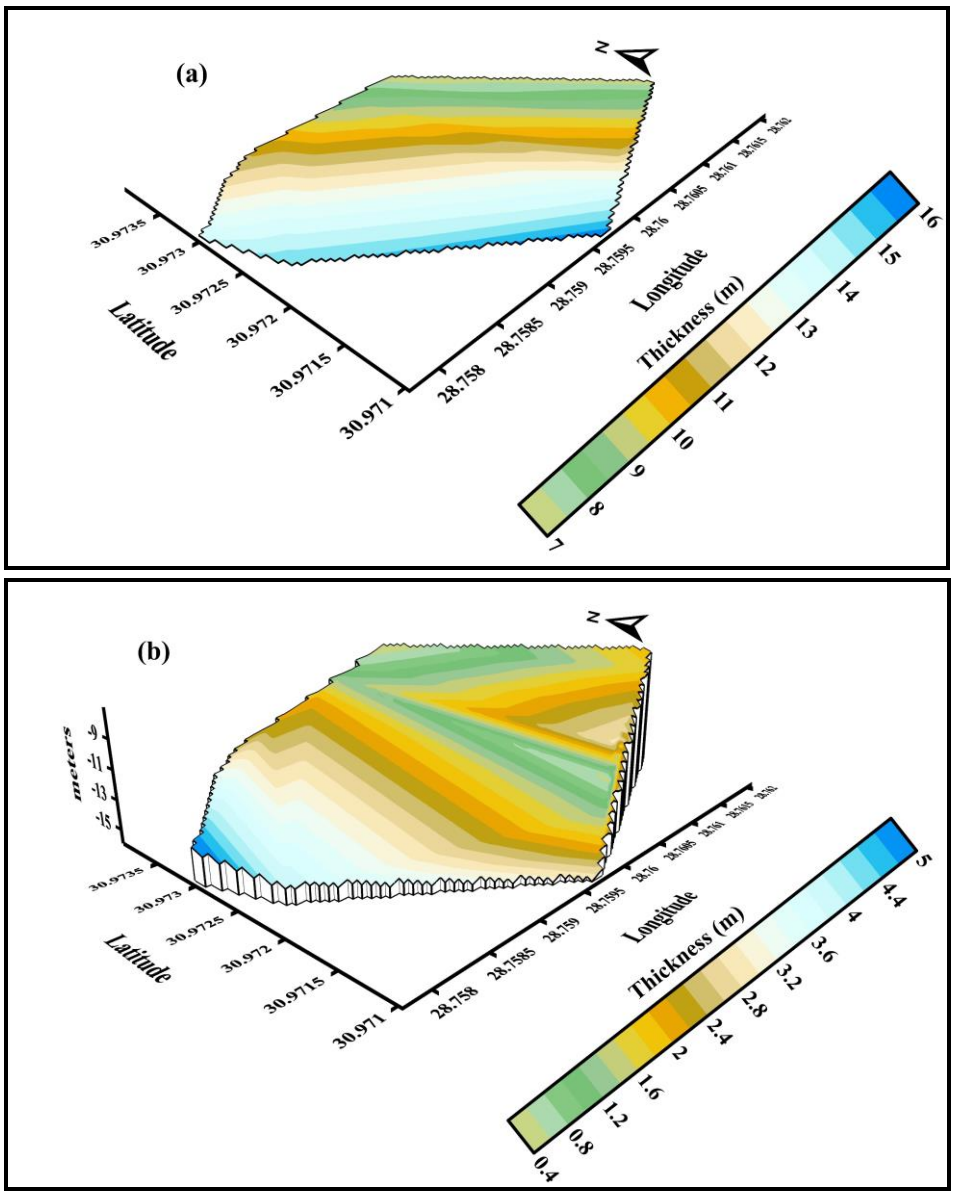

Figure 7: Thickness of (a) top (b) second layers

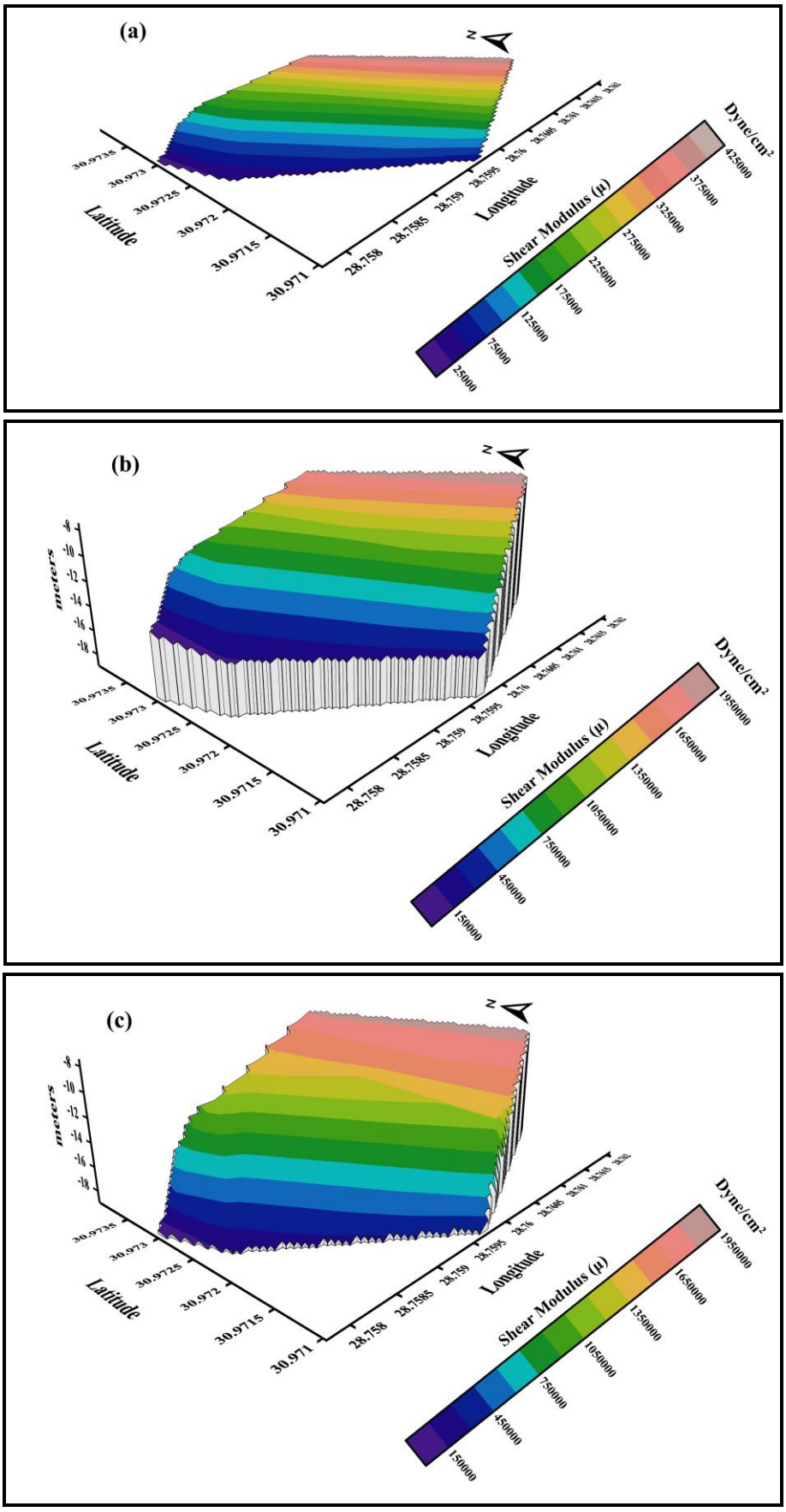

Figure 8: Shear Modulus (μ) distribution for (a) top (b) second (c) third layers.

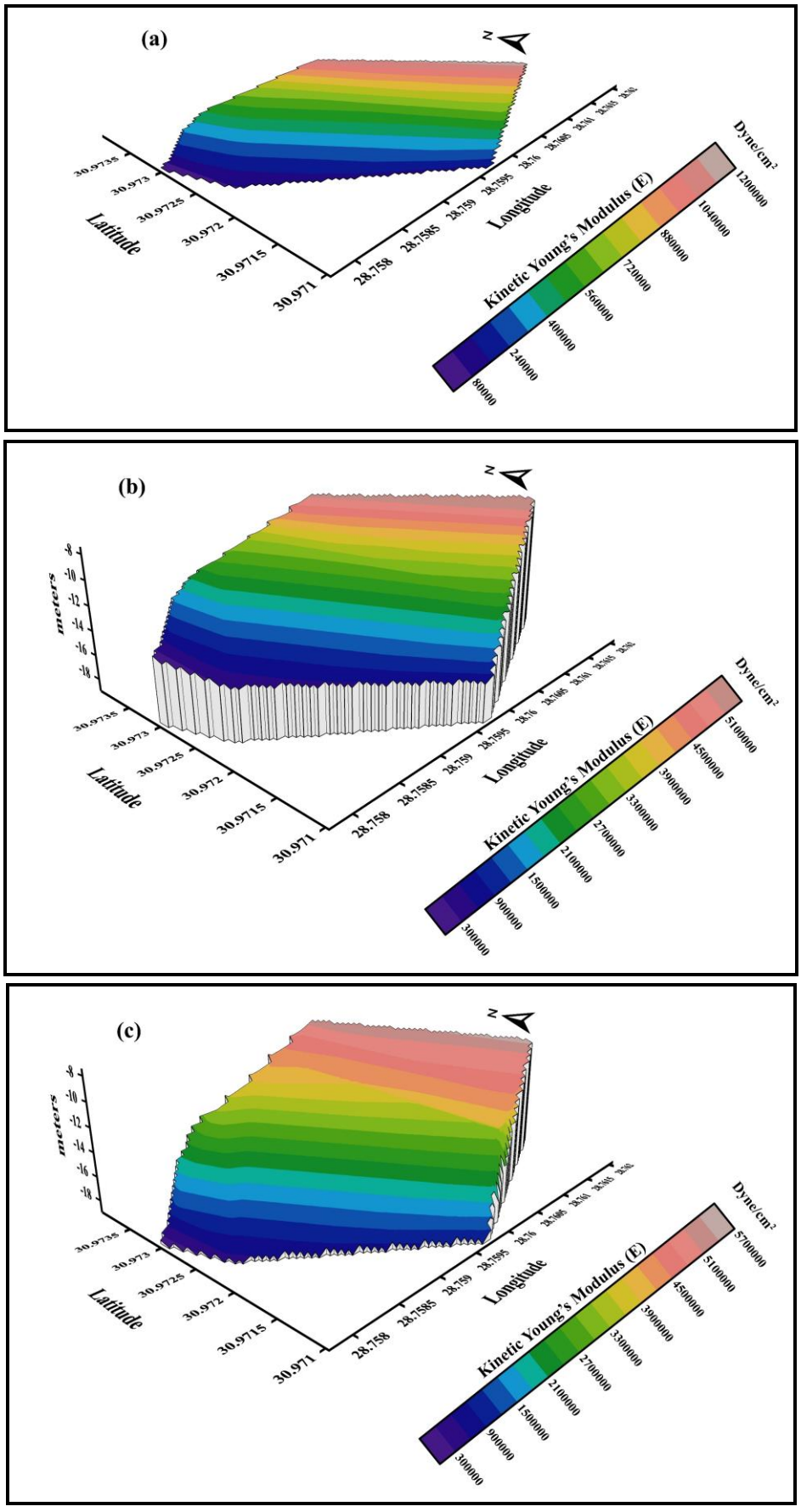

Figure 9: Young's Modulus (E) distribution for (a) top (b) second (c) third layers.

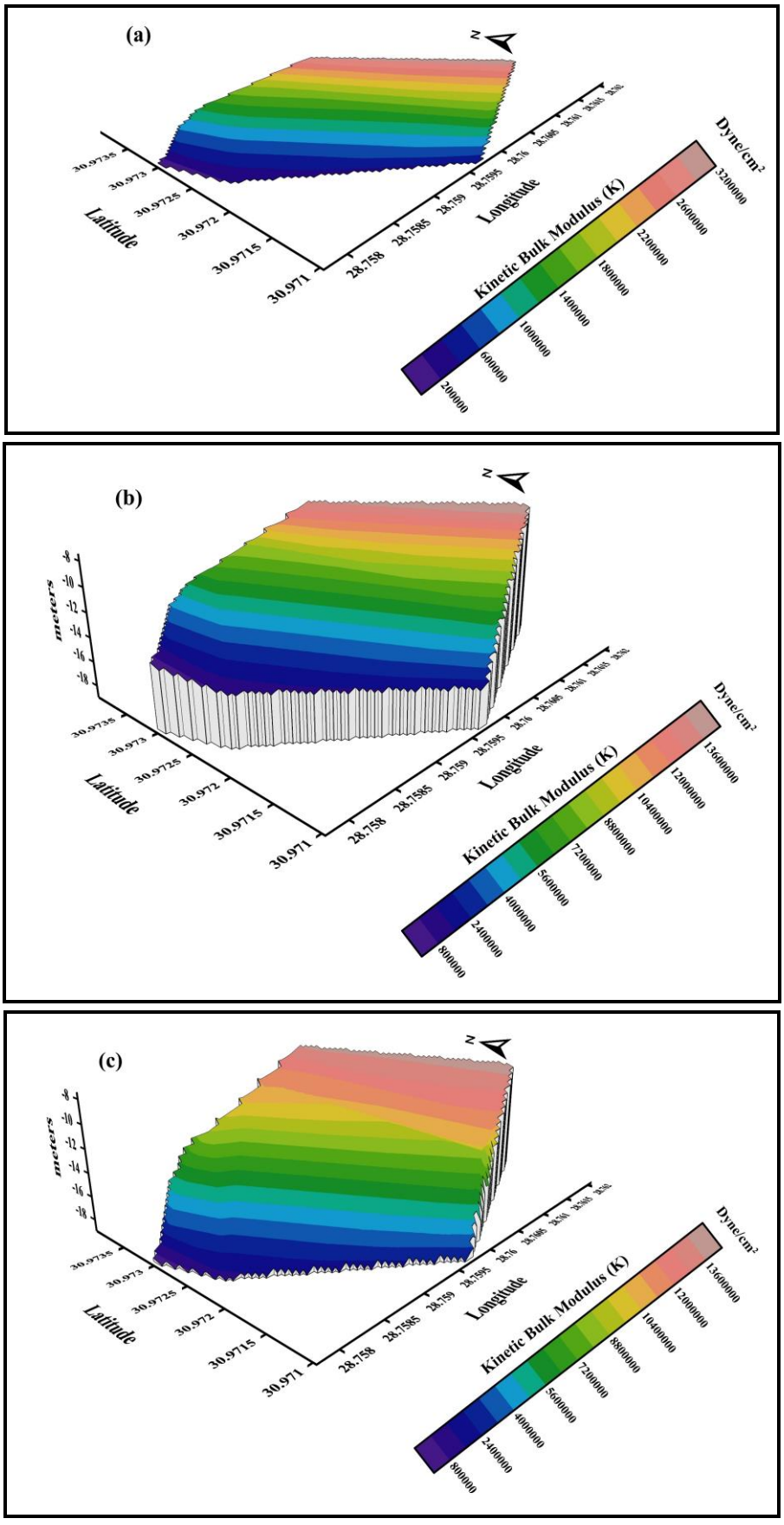

Figure 10: Bulk Modulus (K) distribution for (a) top (b) second (c) third layers

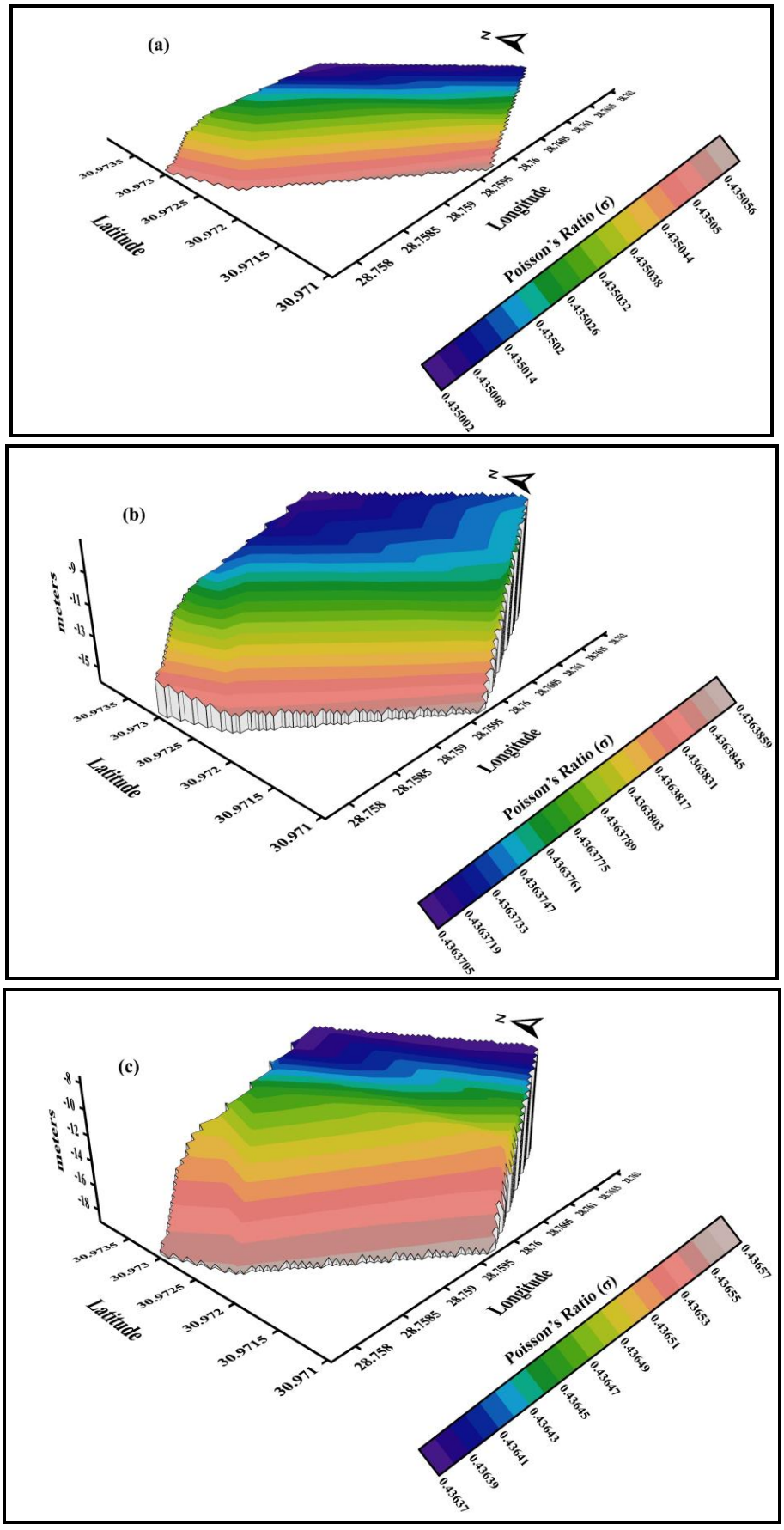

Figure 11: σ distribution for (a) top (b) second (c) third layers.

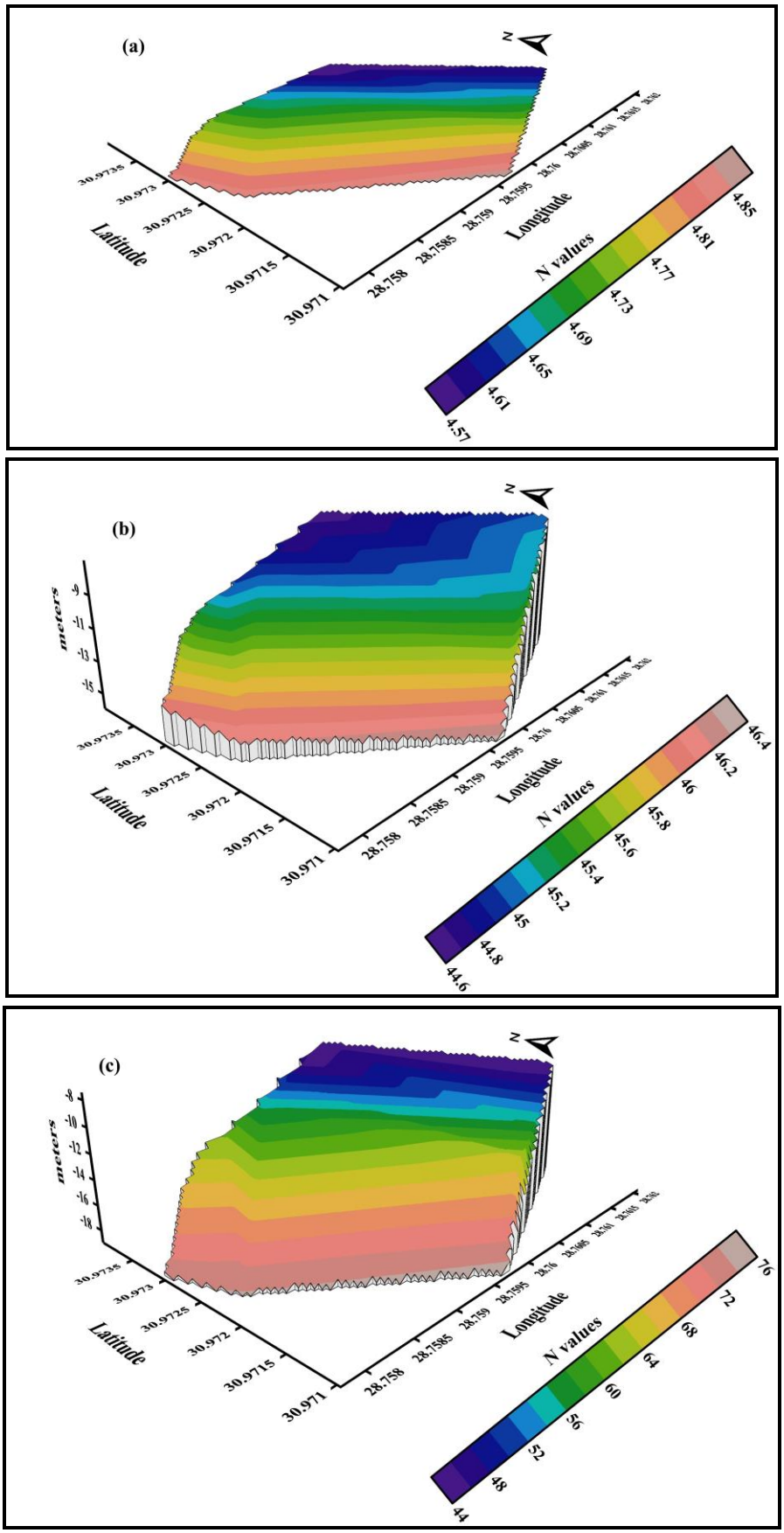

Figure 12: N-value distribution for (a) top (b) second (c) third layers.

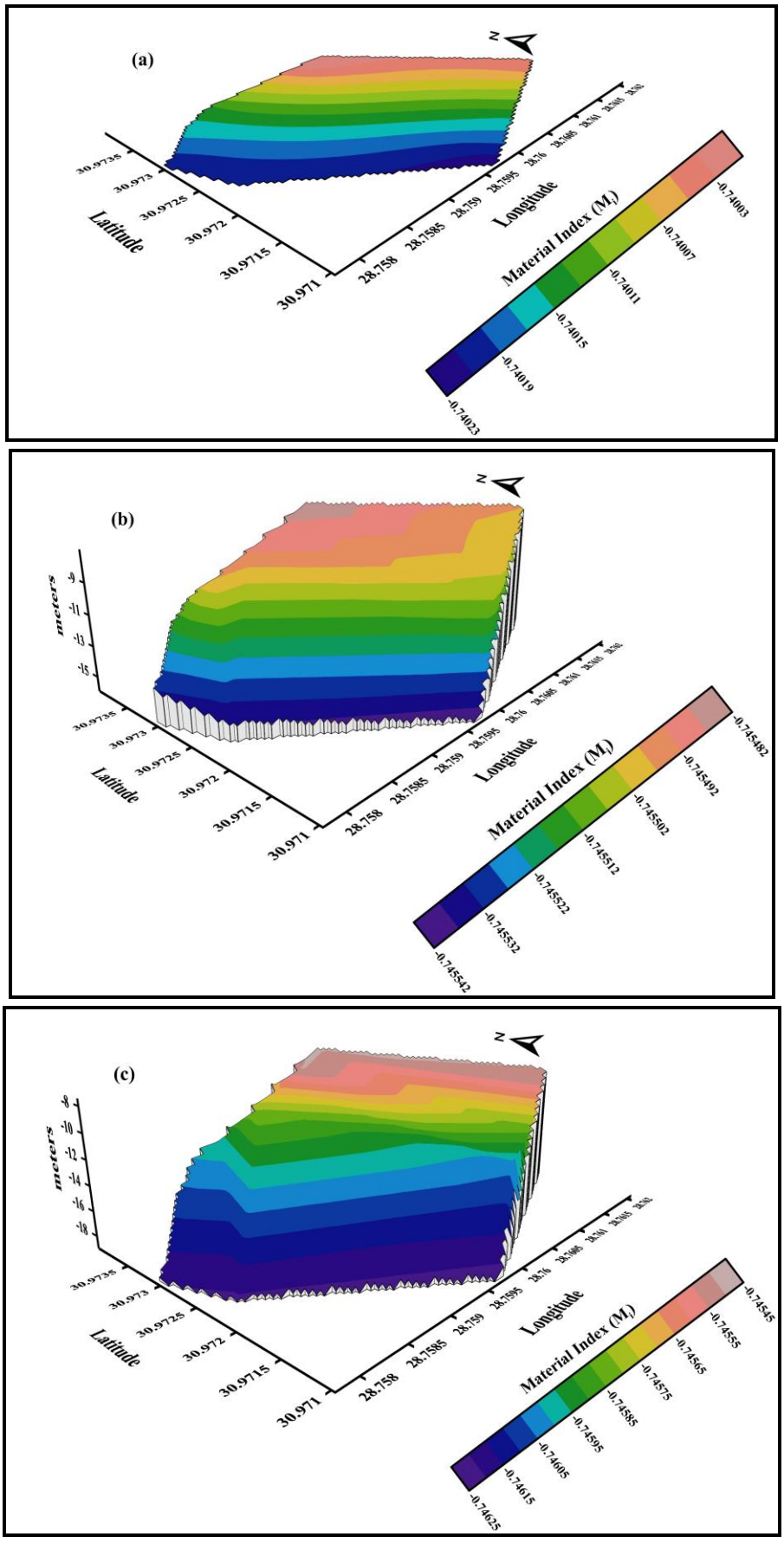

Figure 13: M_i distribution for (a) top (b) second (c) third layers.

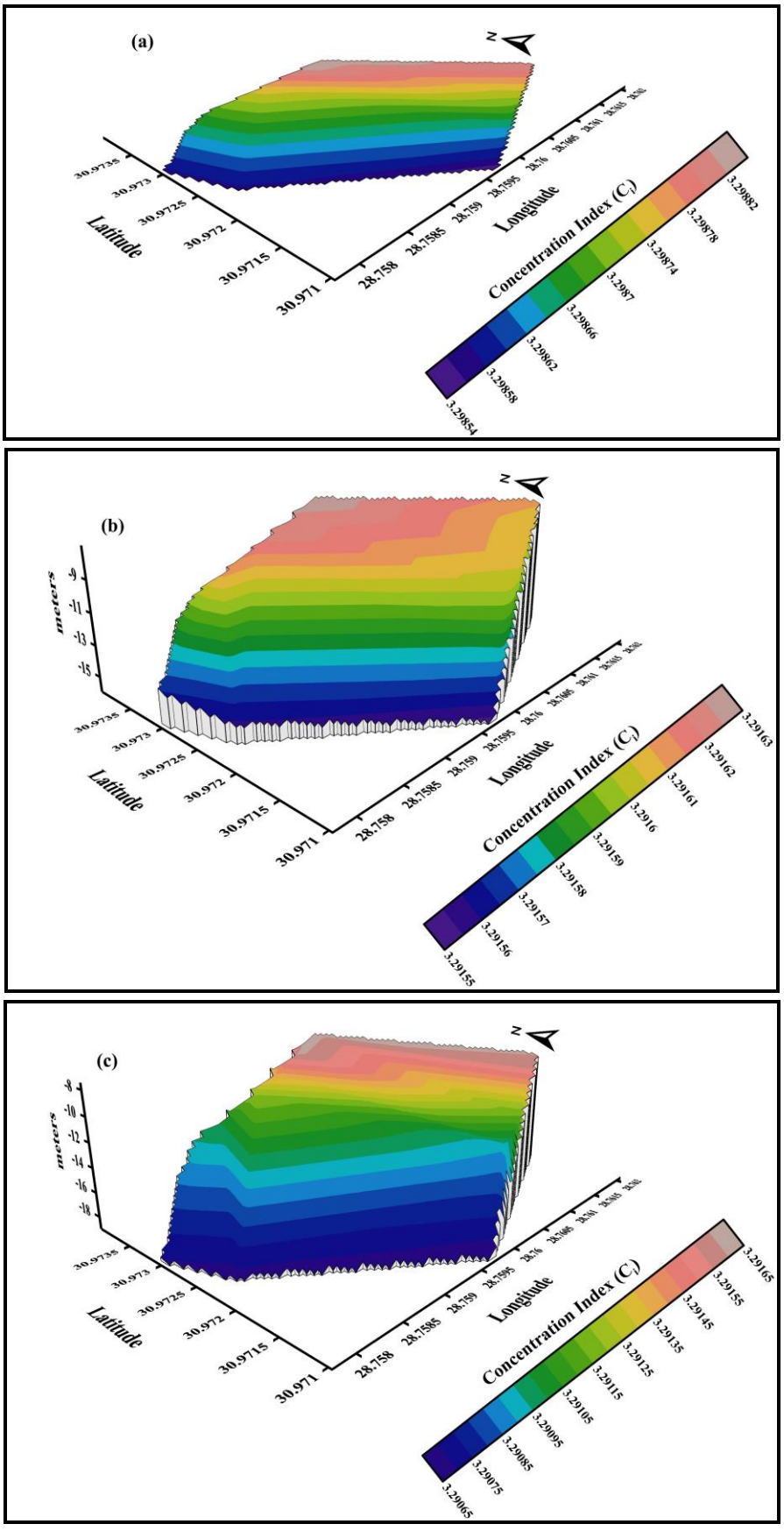

Figure 14: C_i distribution for (a) top (b) second (c) third layers.

4.3.5. Stress Ratio Index (Si)

In general, the stress ratio index values in the study area are very close and high about 0.77 due to the sandy nature of the three layers in the study area and the slight differences are due to the difference in depth and the overlaying vertical load on the various layers (Massarsch et al., 2021; Stapelfeldt et al., 2021; Basheer and Salama, 2022). The low values are observed in the northeastern corners of the three layers and the eastern and southeastern edges of the third layer in the study area. These values gradually increase toward the southwest, west, and northwest directions reaching the maximum values in the southwestern part (Fig. 15). The three layers indicate a less competent material.

4.3.6. Density Gradient (Di)

The relatively low values for the three layers (figs. 16 a-c) observed in the southwestern, western, and northwestern parts of the investigated region indicate more competent materials. High values are observed in the northeastern, eastern, and southeastern corners of the investigated region that reflect less competent materials.

4.4. Foundation bearing capacities

4.4.1. Ultimate bearing capacity (Qult)

The top layer has the lowest ultimate bearing capacity range from 137 to 146 KPa (Fig. 17a). The second layer has a middle ultimate bearing capacity range from 1338.3967 to 1390.8718 KPa (Fig. 17b). The third layer has the highest ultimate bearing capacity ranges from 1338 to 2262 KPa (Fig. 17c). In general, the lowest values are observed in northeastern parts of the surface and second layers while observed in the northeastern, eastern, and southeastern parts of the third layer. These values increase toward southwest, west, and northwest reflecting the presence of the high ultimate bearing capacity materials.

4.4.2. Allowable bearing capacity (Qa)

The surface layer in the study area has the lowest allowable capacity values range from 45.7 to 48.7 KPa (Fig. 18a). The second layer has a middle allowable bearing capacity range from 446 to 463.6 KPa (Fig. 18b). The third layer has the highest allowable bearing capacity that ranges from 446 to 754 KPa (Fig. 18c). For the three layers, the minimum values are detected in northeastern parts of surface and second layers while observed in the northeastern, eastern, and southeastern parts of the third layer. These values increase gradually to the center part until reaching the greatest values in the southwestern, western, and northwestern parts that reflect the highest allowable bearing capacity materials.

As a combined result of the above, based on the results of this work and other previous geotechnical works (Almalki et al., 2011; Khalil and Hanafy, 2016; Khorshid, 2016; Abudeif et al., 2017; Adewoyin et al., 2017; Shebl et al., 2019; Momoh et al., 2020; Ghanem et al., 2021; Basheer and Salama, 2022), It can be found that there is a direct relation between the concentration index, material index, and N value for being low for low competent material and increase as it becomes more competent. Inversely, the stress ratio, Poisson's ratio, and density gradient values are high for low competent material and decrease as it becomes more competent. In other words, the greater values of bearing capacity materials are related to zones having a high material index, high concentration index, high N value, low stress ratio, low Poisson's ratio, and low-density gradient and vice versa (Fig. 19).

Using and integrating the calculated geotechnical parameters, the study area has a relatively low material index (about -0.7), high Poisson's ratio (about 0.43), low concentration index (about 3.3), and high stress ratio (about 0.7). The N value increase from northeastern, eastern, and southeastern corners to southwest, west, and northwest direction, and inversely the density gradient increases from southwestern, western, and northwestern corners to northeast, east, and southeast direction. The entire region is considered a low competent area suitable for a light building and the northwestern, western, and southwestern region is slightly more competent (First region) and less affected by seawater intrusion than the northeastern, eastern, and southeastern region (Second region) (Fig. 20).

Conclusion

This study employed Seismic Refraction Tomography as the primary investigative tool. SRT is a valuable method in engineering investigations for assessing the geotechnical characteristics of rock and sediment formations. The procedure involves seismic wave emission, interaction with geological interfaces, wave reception by geophones placed at the Earth's surface, and analysis of arrival times to convert these travel times into depth values. A comparative study includes comparing the variation between different measured wave speeds, considering the effect of depth, and the lithological sequence of rocks taken from wells drilled and distributed in the study area. Finally, the study area was classified for construction purposes based on the derived geotechnical properties.

The results show that the area can be divided, based on the thickness of the cohesive layers, the amount of soil cohesion derived from the geotechnical properties, and compared to the test wells distributed in the area under investigation, into two regions. The first region is unsuitable for construction due to the weak soil cohesion resulting from the intrusion of seawater into the soil particles. It also features a limited thickness of the layer suitable for building. On the other hand, soil cohesion is good in the second region and there is a considerable layer thickness suitable for construction. Additionally, the interference of seawater is relatively minimal or not uncatchable there.

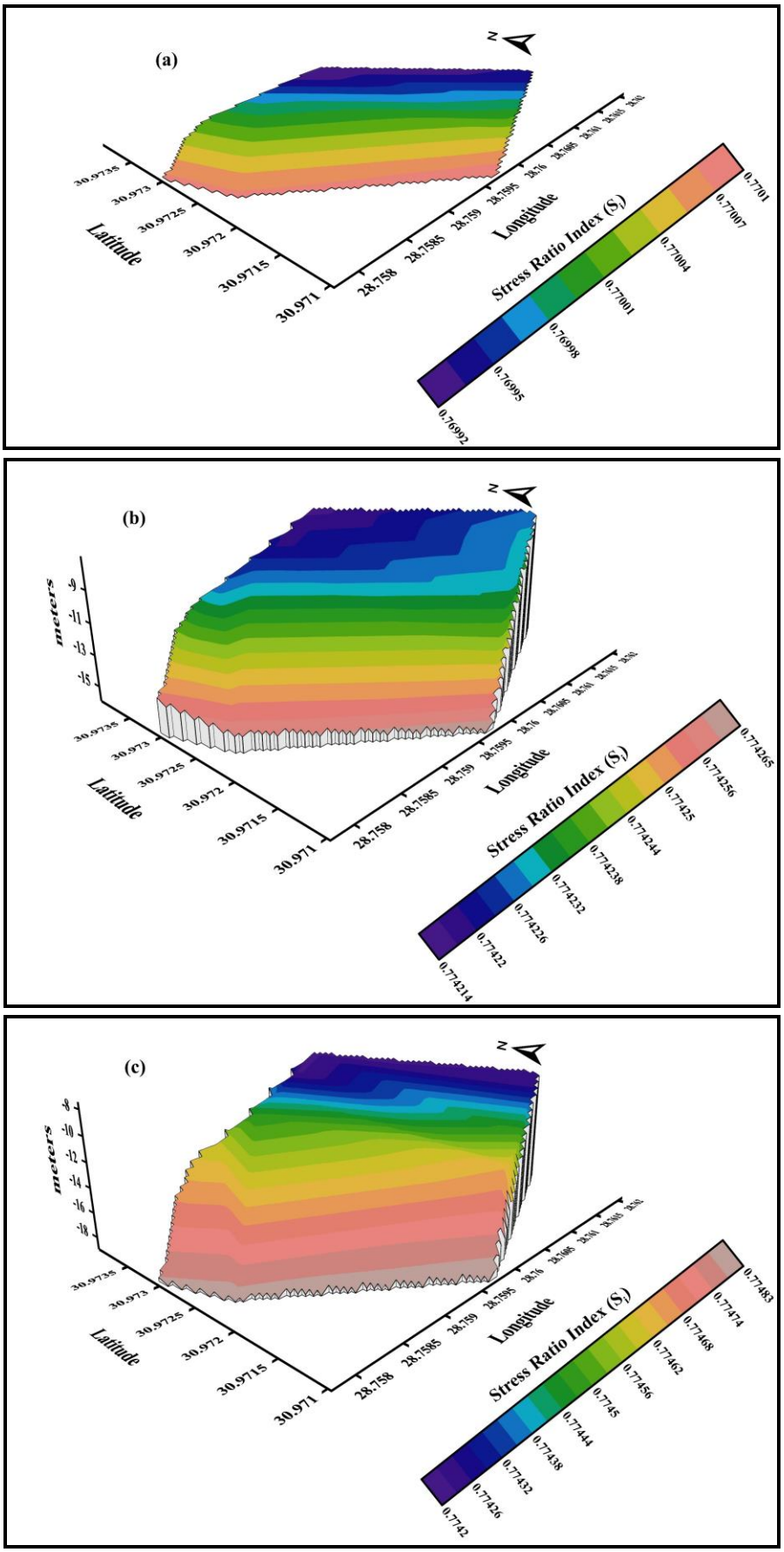

Figure 15: S_i distribution for (a) top (b) second (c) third layers.

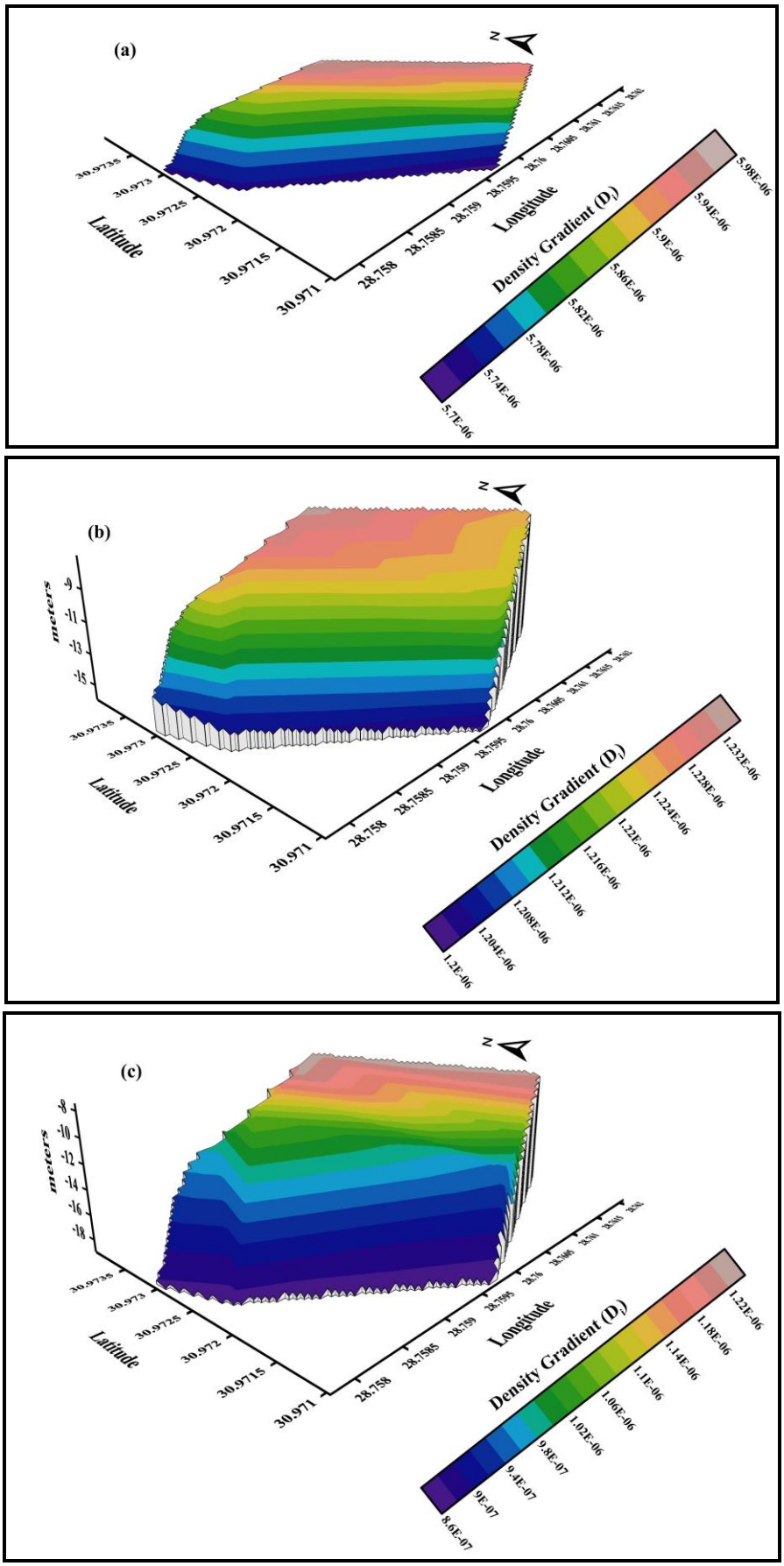

Figure 16: D_i distribution for (a) top (b) second (c) third layers.

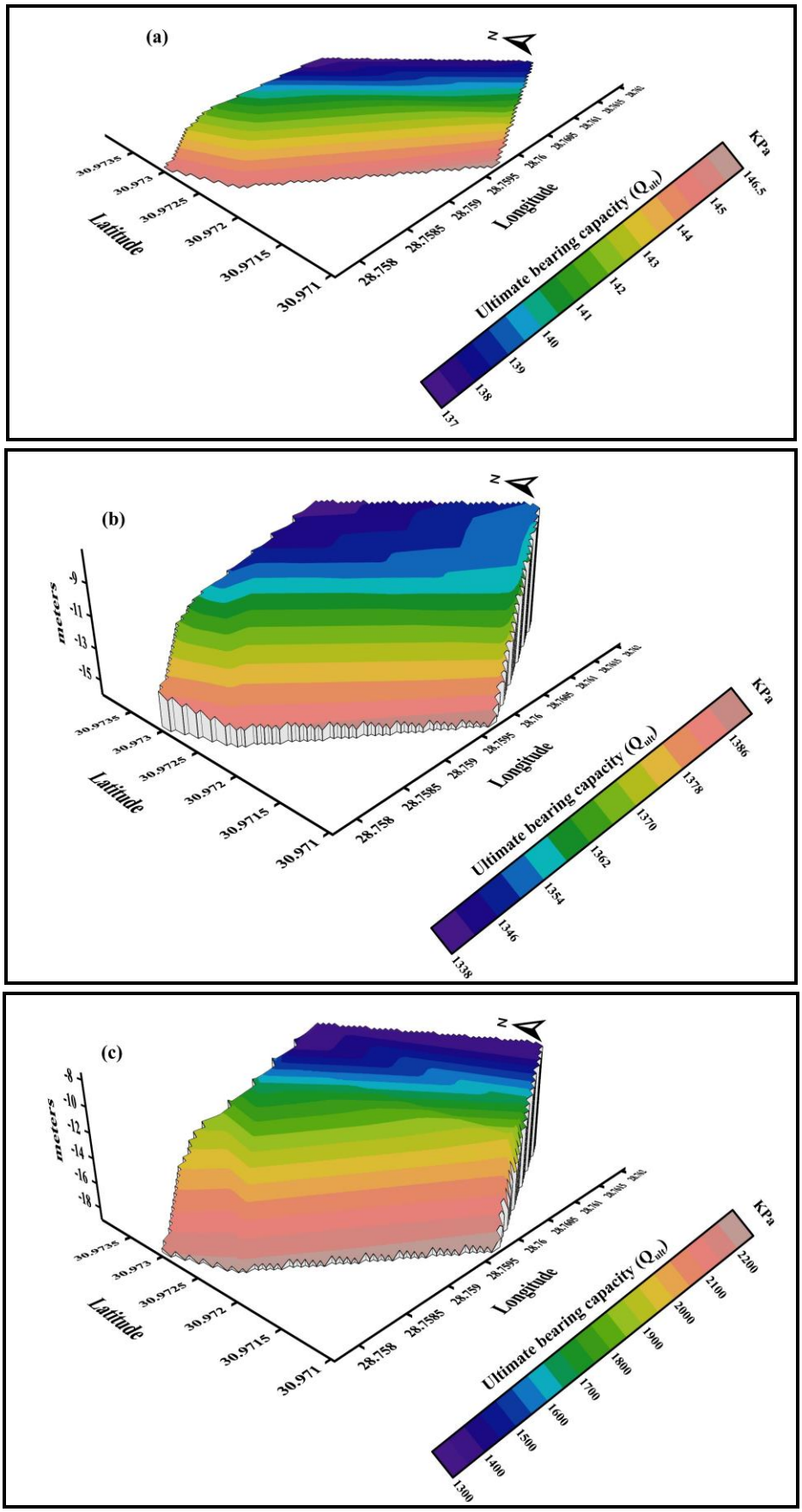

Figure 17: Q_{ult} distribution for (a) top (b) second (c) third layers.

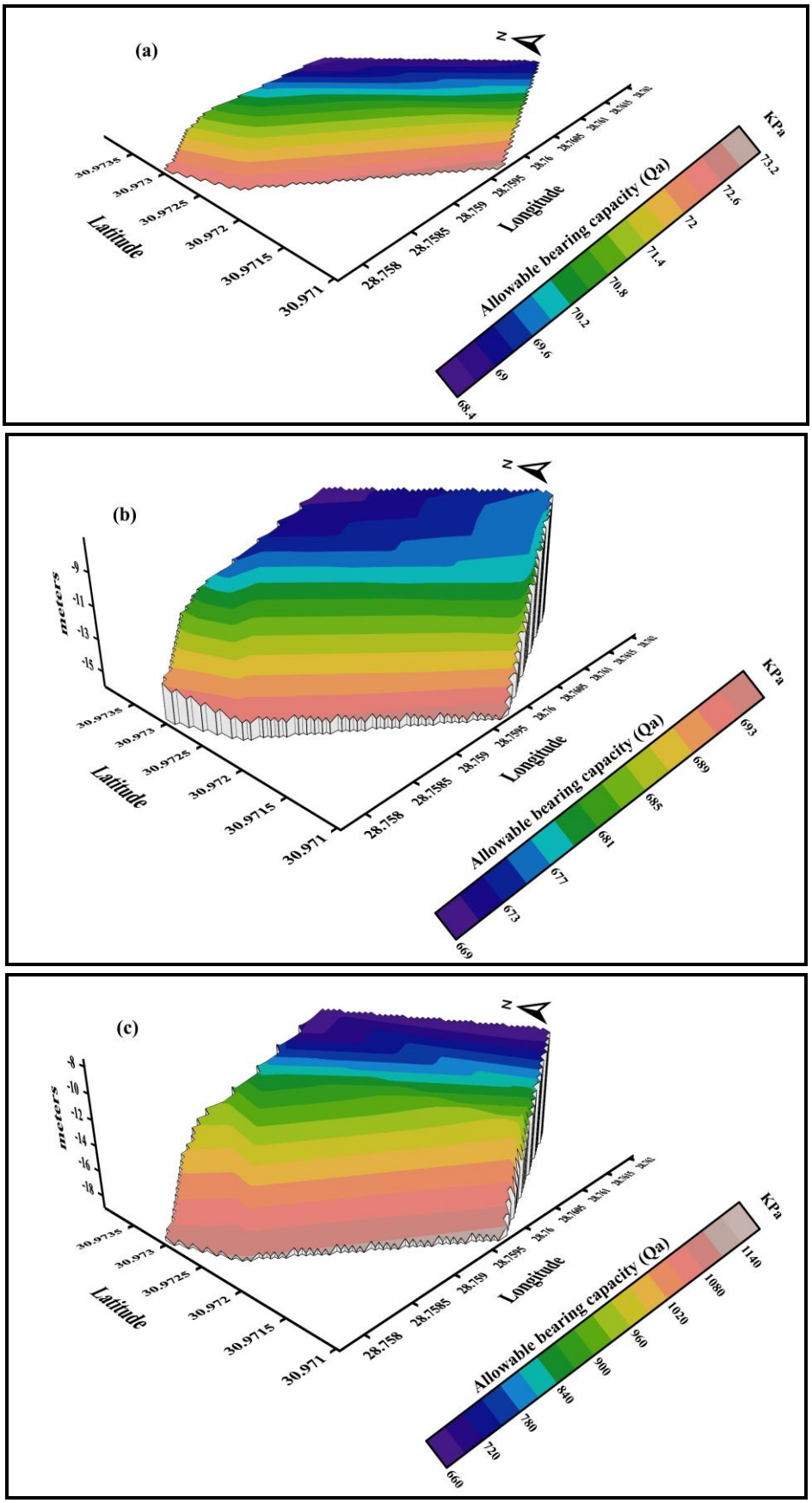

Figure 18: Q_a distribution for (a) top (b) second (c) third layers.

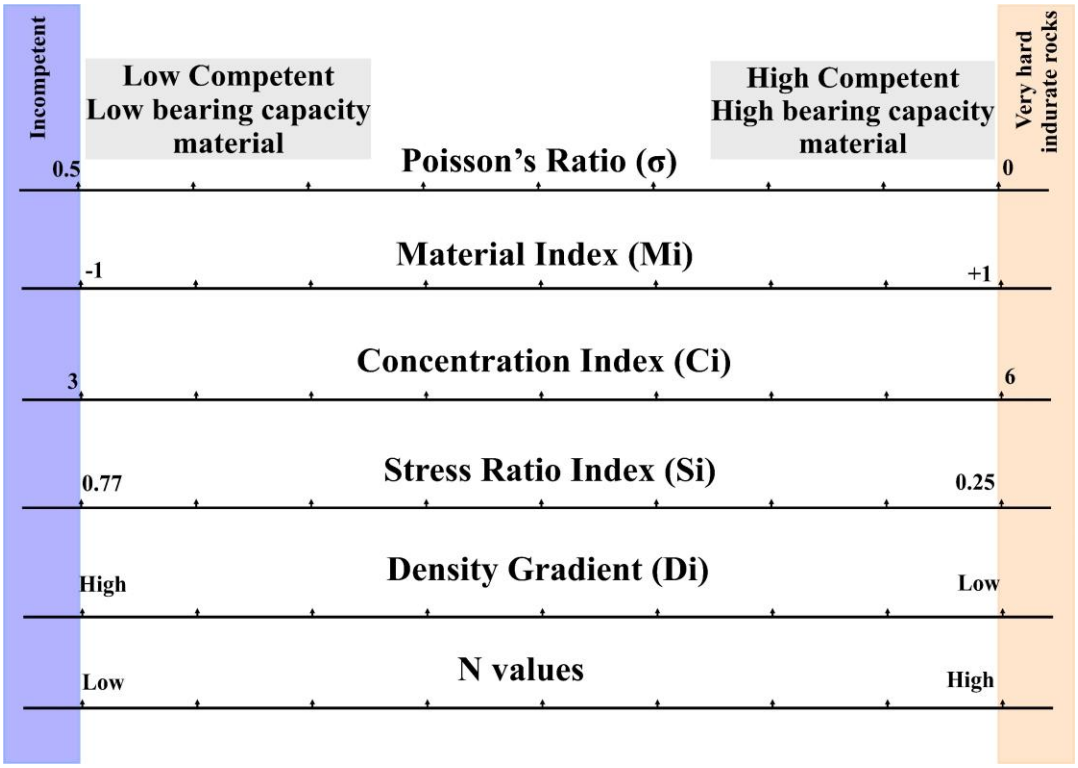

Figure 19: Competence scale based on geotechnical parameters.

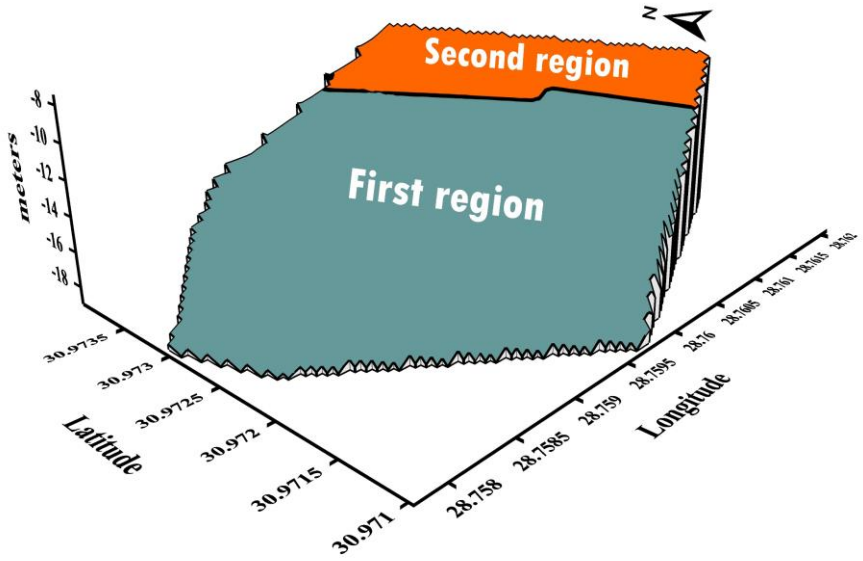

Figure 20: Division of the area for construction purposes.

In a more comprehensive and brief sense, this study's zonal classification based on SRT data serves as a crucial tool for engineers and geotechnical experts, facilitating sound decision-making, risk management, and the development of robust foundation engineering designs in the construction industry. It ultimately contributes to safer and more reliable engineering practices.

Acknowledgments: The authors thank Dr. Nihal Adel, assistant professor in English, Department of English - Faculty of Al-Alsun - Minia University, Egypt for her grammatical and linguistic review of the manuscript research.

References

Abd Elrahman, M. (1989): Evaluation of the Kinetic Elastic Moduli of the Subsurface Material and Application to Engineering Geologic Maps at Ma'Barrisabah area (Dhamar Province), Northern Yeman, Egypt. Journal of geology, vol. 33, no. 1-2, pp. 229-250.

Abd Elrahman, M. M. (1991): Rock material competence assessed by seismic measurements with emphasis on soil competence scale and their applications in some urban areas in Yemen, Egypt. EGS. Proc. of the 9th Ann. Meet, pp. 206-228.

Abd Elrahman, M. M., Setto, I., and El-Werr, A. (1992): Inferring mechanical properties of the foundation material at the 2nd industrial zone, Sadat city, from geophysical measurements. In Egyptian Geophysical Society (EGS), Proceedings of 9th Annual Meeting, pp. 206-228.

Abu Risha, U. A., and Sturchio, N. (2018): The impact of hydrogeological setting on the protection of coastal groundwater aquifers, El Dabaa, Northwestern Coast, Egypt. Journal of Basic and Environmental Sciences, vol. 5, pp. 174-186.

Abudeif, A. M., Raef, A. E., Abdel Moneim, A. A. and Farrag, A. F. (2017): Evaluation of dynamic geotechnical properties and Vs30 of a suggested nuclear power plant site: P- and S-waves seismic refraction surveys, North Western Coast, Egypt. Soil Dynamics and Earthquake Engineering, vol. 99, pp. 124-136.

https://doi.org/10.1016/j.soildyn.2017.05.006.

Adewoyin, O. O., Joshua1, E. O., Akinwumi, I. I., Omeje1, M. and Joel, E. S. (2017): Evaluation of Geotechnical Parameters using Geophysical Data. Journal of Engineering and Technological Sciences, vol. 49, no. 1, pp. 95-113.

https://doi.org/10.5614/j.eng.technol.sci.2017.49.1.6

Al-Fahdawi, S. S. j. (2000): The Use of Seismic Refraction and CrossHole Methods for Geotechnical Evaluation of Engineering Site in Al-Madain Archaeological Area – South Baghdad. Unpublished M.Sc. Thesis, Collage of Science, Baghdad University, p.165.

Al-Heety, A. (2014): Seismic Refraction Survey for Teaching Hospital Project site of the Mosul University. University of Mosul, College of Science, Master Thesis, p. 126.

Al-Heety, A. J. R., Hassouneh, M. and Abdullah, F. M. (2021): Application of MASW and ERT methods for geotechnical site characterization: A case study for roads construction and infrastructure assessment in Abu Dhabi, UAE. Journal of Applied Geophysics, vol. 193, pp. 104408.

https://doi.org/10.1016/j.ijrmms.2019.04.018

Almalki, H., El-Werr, A. and Abdel-Rahman, K. (2011): Estimation of near-surface geotechnical parameters using seismic measurements at the proposed KACST expansion site, Riyadh, KSA. Arab Journal of Geoscience, vol. 4, pp. 1131–1150. https://doi.org/10.1007/s12517-010-0124-3.

AL-Zubedi, A. S. (2020): Principles of seismic refraction method. published by araa for printing and publishing, Baghdad, p. 76. ISBN: 978-9922-9346-0-0.

Atwa, S. M. M. (1979): Hydrogeology and hydrogeochemistry of the western coast of Egypt. Ph.D. Thesis, Faculty of Science, Alexandria University, Egypt.

Basheer, A. A. and Salama, N. S. (2022): Application of ERT and SSR for geotechnical site characterization: A case study for resort assessment in New El Alamein City, Egypt. NRIAG journal of astronomy and geophysics, vol. 11, no. 1, pp. 58–68. https://doi.org/10.1080/20909977.2021.2023999

Basu, D., Salgado, R. and Prezzi, M. (2008): Analysis of laterally loaded piles in multilayered soil deposits. Joint Transport Res Program vol. 23, pp. 330. https://doi.org/10.5703/1288284313454

Biot, M. A. (1956): Theory of propagation of elastic waves in a fluid-saturated porous solid. The Journal of the acoustical Society of america, vol. 28, no. 2, pp. 179-191.

https://doi.org/10.1121/1.1908241

Birch, F. (1966): Handbook of physical constants. Geol. Soc. Amer. Men., p. 613.

Bowles, J. E. (1982): Foundation Analysis and Design (2nd edition). McGraw-Hill International Book Company, London, p. 587.

Bowles, J. E. (1984): Physical and geotechnical properties of soils. Mc Graw-Hill, London, p. 478.

Butzer, K. W. (1960): On the Pleistocene shorelines of Arabs' Gulf. The Journal of Geology, vol. 68, no. 6, pp. 626-637. https://doi.org/10.1086/626701

Cordier, J. P. (1985): Velocities in Refraction Seismology. Radial Publisher Company, Holland, p. 276.

Cosenza, P., Marmet, E., Rejiba, F., Cui, Y. J., Tabbagh, A. and Charlery, Y. (2006): Correlations between geotechnical and electrical data: a case study at Garchy in France. Journal of Applied Geophysics, vol. 60, no. 3-4, pp. 165-178.

D'Andrea, D. V., Fisher, R. L., and Fagelaon, D. E. (1965): Prediction of Compressive Strength From other Rock properties. U.S. Department of the Interior, Bureau of Mines, Washington, USA, vol. 6702, p. 23.

Das, B.M. (1994): Principles of Geotechnical Engineering. PWS Publishing Company, USA, p. 766.

Dewidar, K. M., and Frihy, O. E. (2010): Automated techniques for quantification of beach change rates using Landsat series along the North-eastern Nile Delta, Egypt. Journal of Oceanography and Marine Science, vol. 1, no. 2, pp. 028-039.

Dobrin, M. B. (1976): Introduction to Geophysical Prospecting (3rd edition). New York: McGraw Hill Book, p. 630.

Elstohey, A. S., El-Tahhan, M. K., Elsayed, W. R. and Moghazy, H. M. (2023): Assessment shoreline changes of El Alamein and Marina coastal area, northwestern coast of Egypt. Alexandria Engineering Journal, vol. 67, pp. 655-671.

Gassman, F. (1973): Seismische Prospektion. Birkhaeuser, Stuttgart, p. 417.

Geertsma, J. (1961): Velocity-log interpretation: The effect of rock bulk compressibility. Society of Petroleum Engineers Journal, vol. 1, no. 04, pp. 235-248. https://doi.org/10.2118/1535-G

Ghanem, F. K., Al Amoush, H. and Al-Tarazi, E. (2021): Geotechnical Engineering Evaluation of Superficial Deposits Utilizing Seismic Methods at Al al-Bayt University, Jordan. Iraqi Geological Journal, vol. 54, pp. 11-28.

Gregory, A. R. (1976): Fluid saturation effects on dynamic elastic properties of sedimentary rocks. Geophysics, vol. 41, no. 5, pp. 895-921. https://doi.org/10.1190/1.1440671

Gretener, P. (2003): Summary of the Poisson's Ratio debate 1990–2003. Feature Article, CSEG Recorder, vol. 28, no. 7, pp. 44-45.

Gupta, B. K. and Basu, D. (2017): Analysis of laterally loaded short and long piles in multilayered heterogeneous elastic soil. Soils Found vol. 57(1), pp. 92–110.

https://doi.org/10.1016/j.sandf.2017.01.007.

Hamilton, E. L. (1971): Elastic properties of marine sediments. Journal of geophysical research, vol. 76, no.2, pp. 579-604. https://doi.org/10.1029/JB076i002p00579

Hammad, F. A. (1966): The geology of water supplies in Ras El Hekma area. M. Sc. Thesis, Faculty of Science, Cairo University, p. 109.

Hardin, B. O. and Dmevich, V. P. (1972): Shear modulus and damping in soils: Measurement and parameter effects. Journal of the soil mechanics and foundations division, vol. 98, no. 6, pp. 603-624. https://doi.org/10.1061/JSFEAQ.0001756

Hubbard, J. L. (2009): Use of Electrical Resistivity and Multichannel Analysis Of Surface Wave Geophysical Tomography in Geotechnical Site Characterization of Dam. MSc dissertation. The University of Texas at Arlington.

Hume W. E., and Hughes F. (1921): The soils and water supply of the Maryut district, west of Alexandria. Government press, no. 37.

Hunt, R. E. (1986): Geotechnical Engineering Analysis and Evaluation. McGraw-Hill book company, p. 730.

Imai, S. (1975): An investigation to geophysical prospecting for civil purposes. OYO Corporation, Tokyo, Japan, pp. 17-34.

Iskander, M. M. (2013): Wave climate and coastal structures in the Nile Delta coast of Egypt. Emirates Journal for Engineering Research, vol. 18, no. 1, pp. 43-57.

Iskander, M. M. (2021): Stability of the Northern coast of Egypt under the effect of urbanization and climate change. Water Science, vol. 35, no. 1, pp. 1-10.

Kearey, P., Brooks, M., and Hill, I. (2002): An Introduction to Geophysical Exploration. John Wiley and Sons, vol. 4, p. 288.

Khalil, M. H. and Hanafy, S. M. (2008): Engineering applications of geophysics: A field example at Wadi Wardan, northeast Gulf of Suez, Sinai, Egypt. Journal of Applied Geophysics, vol. 65, no. 3-4, pp. 132–141. https://doi.org/10.1016/j.jappgeo. 2008.06.003

Khalil, M. H. and Hanafy, S. M. (2016): Geotechnical Parameters from Seismic Measurements: Two Field Examples from Egypt and Saudi Arabia. Journal of Environmental and Engineering Geophysics, vol. 21, Issue 1, pp. 13–28.

https://doi.org/10.2113/JEEG21.1.13.

Khorshid, S. Z. A. (2016): Determination of Elastic Moduli and Geotechnical Parameters of the Upper Soil Layer Using Ultrasonic Waves in Al- Jadiriyah Area - University of Baghdad-Iraq. Iraqi Journal of Science, 2016, Vol. 57, No.4C, pp: 2909-2921.

Koukis, G., Sabatakakis, N. and Papanakli, S. (2007): Laboratory testing properties of sandstones. Bulletin of the Geological Society of Greece, vol. 40, no. 4, pp. 1695-1702.

https://doi.org/10.12681/bgsg.17083

Kuster, G. T., and Toksoz (1974): Velocity and attenuation of seismic waves in two phase media. Geophysics, vol. 39, no. 5, pp. 587-606. https://doi.org/10.1190/1.1440450

Lowrie, W. (2007): Fundamentals of Geophysics, 2nd Edn. The United States of America, New York, Cambridge University Press.

Massarsch, K. R., Wersäll, C. and Fellenius, B. H. (2021): Liquefaction induced by deep vertical vibratory compaction. Proc Inst Civil Engineers-Ground Improv, vol. 174(3), pp. 194–205. https://doi.org/10.1680/jgrim.19.00018.

Momoh, K. O., Muhammad, U. I., Usman, A. and Ibrahim, A. U. (2020): Estimation of near-surface geotechnical parameters using seismic measurements at phase II site, Ahmadu Bello University Zaria, North-western Nigeria. Global Journal of Earth and Environmental Science, vol. 5, no. 1, pp. 1-10.

https://doi.org/10.31248/GJEES2019.052

Mott, P. H., Dorgan, J. R., and Roland, C. M. (2008): The bulk modulus and Poisson's ratio of "incompressible" materials. Journal of Sound and Vibration, vol. 312, no. 4-5 pp. 572–575. https://doi.org/10.1016/j.jsv.2008.01.026

Nur, A., and Simmons, G. (1969): Stress-induced velocity anisotropy in rock-An experimental study. Journal of Geophysical Research, vol. 74, no. 27, pp. 6667-6674.

https://doi.org/10.1029/JB074i027p06667

Othman, A. A. A. (2005): Construed geotechnical characteristics of foundation beds by seismic measurements, Journal of Geophysics and Engineering, vol. 2(2), pp. 10-11. https://doi.org/10.1088/1742 2132/2/2/007.

Parry, R. H. G. (1977): Estimating bearing capacity of sand from SPT values. JGED ASCE, vol. 103, issue 9, pp. 1014–1043. https://doi.org/10.1061/AJGEB6.0000484

Potter, C. C. and Fottinek, D. S. (1997): Formation Elastic Parameters by Deriving S- Wave Velocity Logs. CREWS Research Report, vol. 9, pp. 10-23.

Qaher, M., Eldosouky, A. M., Saada, S. A. and Basheer, A. A. (2023): Integration of ERT and shallow seismic refraction for geotechnical investigation on El-Alamein Hotel Building Area, El-Alamein new city, Egypt. Geomechanics and Geophysics for Geo-Energy and Geo-Resources, vol. 9, no. 115, pp. 1-23. https://doi.org/10.1007/s40948-023-00639-8.

Rahmouni, A., El rhaffari, y., Boulanouar, a., Samaouali1, a., Boukalouch, m., Géraud, y. and sebbani, m. j. e. (2017): Effect of porosity and water saturation on the mechanical properties and P-wave velocity of calcarenite rocks used in the construction of historical monuments of Rabat (Morocco). 13ème Congrès de Mécanique (Meknès, MAROC), vol. 7, no. 1, pp. 1-3.

Said, R. (1962): The Geology of Egypt. Elsevier Pub. Co., Amsterdam and New York, p. 377.

Said, R. (1990): The Geology of Egypt. Balkema-Rotterdam-Brook field, USA, p. 734.

Saleh, S., Jahr, T., Jentzsch, G., Saleh, A. and Abou Ashour, N. M. (2006): Crustal evaluation of the northern Red Sea rift and Gulf of Suez, Egypt from geophysical data: 3-dimensional modeling. Journal of African Earth Sciences, vol. 45, no. 3, pp. 257-278.

Saleh, S., Jahr, T., Jentzsch, G., Saleh, A. and Abou Ashour, N. M. (2006): Crustal evaluation of the northern Red Sea rift and Gulf of Suez, Egypt from geophysical data: 3-dimensional modeling. Journal of African Earth Sciences, vol. 45, no. 3, pp. 257-278.

Salem, H. (1990): A Theoretical and Practical Study of Petrophysical, Electric and Elastic Parameters of Sediments, Ph.D. Thesis, Kiel University, Germany, Publish by University Microfilms International (UMI), USA, p. 200.

Salem, M., Elmamlouk, H. and Agaiby, S. (2013): Static and cyclic behavior of North Coast calcareous sand in Egypt. Soil Dynamics and Earthquake Engineering, vol. 55, pp. 83-91.

Samui, P. and Sitharam, T. (2010): Correlation between SPT, CPT and MASW. International Journal of Geotechnical Engineering, vol. 4, no. 2, pp. 279–288.

https://doi.org/10.3328/IJGE.2010.04.02.279-288.

Schlumberger (1984): Geology of Egypt. Well evaluation conference of Egypt, Schlumberger Middle East Service, pp. 1-64.

Shaaban, F. A. (2004): Geophysical evaluation of the groundwater potentiality, southeast Matrouh area, Egypt. NRIAG Journal of Geophysics, Special Issue, pp. 243-266.

Sharma, P. V. (1997): Environmental and Engineering Geophysics. Cambridge University Press, Cambridge, p. 475.

Shata, A. A. (1971): The geomorphology, pedology and hydrogeology of the Mediterranean coastal desert of the UAR. In Symposium on the Geology of Libya, pp. 431-436.

Shebl, S., Gemail, K. S., Attwa, M., Soliman, S. A., Azab, A. and Farag, M.H. (2019): Utilizing shallow seismic refraction in defining the geotechnical properties of the foundation materials: A case study at New Minia City, Nile Valley, Egypt. Egyptian Journal of Petroleum, vol. 28, Issue 2, pp. 145-154. https://doi.org/10.1016/j.ejpe.2018.12.006

Sheriff, R. E. (1991): Encyclopedic dictionary of exploration geophysics (3rd edition). Society of Exploration Geophysicists, p. 442.

Sheriff, R. E. and Geldart, L. P. (1995): Exploration Seismology. Cambridge Univ. Press, Cambridge, p. 316.

Shipton, B. and Coop, M. R. (2015): Transitional behaviour in sands with plastic and non-plastic fines. Soils and Foundations, vol. 55, no. 1, pp. 1-16.

https://doi.org/10.1016/j.sandf.2014.12.001.

Shukri, N. M., Philip, G. and Said, R. (1956): The geology of the Mediterranean coast between Rosetta and Bardia. Part II: Pleistocene sediments; geomorphology and microfacies. Bulletin Institute of d'Egypte, vol. 37, no. 2, pp. 395-427.

Sjogren, B. (1984): Shallow Refraction Seismics. Chapman and Hall., London, p. 268. http://dx.doi.org/10.1007/978-94-009-5546-2

Stapelfeldt, M., Bienen, B. and Grabe, J. (2021): Influence of low-permeability layers on the installation and the response to vertical cyclic loading of suction caissons. Journal of Geotechnical and Geoenvironmental Engineering, vol. 147, no. 8, pp. 04021076. https://doi.org/10.1061/(ASCE)GT.1943-5606.0002522.

Stumpel, H., Kahler, S., Meissner, R. and Milkerei, B. (1984): The use of seismic shear waves and compressional waves for lithological problems of shallow sediments. Geoph. Pros. Vol. 32, pp. 660-675. https://doi.org/10.1111/j.1365-2478.1984.tb01712.x.

Tatham, R. H. (1982): Vp/Vs and lithology. Geophysics, vol. 47, no. 3, pp. 336-344. https://doi.org/10.1190/1.1441339

Telford, W. M., Geldart, L. P., and Sheriff, R. E. (1990): Resistivity Methods, In: Applied Geophysics, (2nd Edition). Cambridge Univ. Press, Cambridge, UK, p. 751.

Terzaghi, K. (1943): Theoretical soil mechanics. John Weller and sons, Inc. London.

Thomsen, L. (1986): Weak elastic anisotropy. Geophysics, vol. 51, pp. 1954-1966.

Toksöz, M. N., Cheng, C. H., and Timur, A. (1976): Velocities of seismic waves in porous rocks. Geophysics, vol. 41, pp. 621–645. https://doi.org/10.1190/1.1440639

Yousif, M., El Abd, S. and Baraka, A. (2013): Assessment of water resources in some drainage basins, northwestern coast, Egypt. Appl Water Sci, vol. 3, pp. 439-452.

https://doi.org/10.1007/s13201-013-0093-2.